Evolutionary Ecology Research, 2012, **14**: 555–582

Evolutionary-branching lines and areas in bivariate trait spaces

Hiroshi C. Ito[1,2] and Ulf Dieckmann[1]

[1]*Evolution and Ecology Program, International Institute for Applied Systems Analysis (IIASA), Laxenburg, Austria and* [2]*Department of Evolutionary Studies of Biosystems, The Graduate University for Advanced Studies (Sokendai), Hayama, Kanagawa, Japan*

ABSTRACT

Aims: Evolutionary branching is a process of evolutionary diversification induced by frequency-dependent ecological interaction. Here we show how to predict the occurrence of evolutionary branching in bivariate traits when populations are evolving directionally.

Methods: Following adaptive dynamics theory, we assume low mutation rates and small mutational step sizes. On this basis, we generalize conditions for evolutionary-branching points to conditions for evolutionary-branching lines and areas, which delineate regions of trait space in which evolutionary branching can be expected despite populations still evolving directionally along these lines and within these areas. To assess the quality of predictions provided by our new conditions for evolutionary-branching lines and areas, we analyse three eco-evolutionary models with bivariate trait spaces, comparing the predicted evolutionary-branching lines and areas with actual occurrences of evolutionary branching in numerically calculated evolutionary dynamics. In the three examples, a phenotype's fitness is affected by frequency-dependent resource competition and/or predator–prey interaction.

Conclusions: In the limit of infinitesimal mutational step sizes, evolutionary branching in bivariate trait spaces can occur only at evolutionary-branching points, i.e. where the evolving population experiences disruptive selection in the absence of any directional selection. In contrast, when mutational step sizes are finite, evolutionary branching can occur also along evolutionary-branching lines, i.e. where disruptive selection orthogonal to these lines is sufficiently strong relative to directional selection along them. Moreover, such evolutionary-branching lines are embedded in evolutionary-branching areas, which delineate all bivariate trait combinations for which evolutionary branching can occur when mutation rates are low, while mutational step sizes are finite. Our analyses show that evolutionary-branching lines and areas are good indicators of evolutionary branching in directionally evolving populations. We also demonstrate that not all evolutionary-branching lines and areas contain evolutionary-branching points, so evolutionary branching is possible even in trait spaces that contain no evolutionary-branching point at all.

Keywords: adaptive dynamics, frequency-dependent selection, predator–prey interaction, resource competition, two-dimensional trait space.

Correspondence: H.C. Ito, Department of Evolutionary Studies of Biosystems, The Graduate University for Advanced Studies (Sokendai), Hayama 240-0193, Kanagawa, Japan. e-mail: hiroshibeetle@gmail.com

INTRODUCTION

Evolutionary branching is a process of evolutionary diversification induced by ecological interaction (Metz *et al.*, 1992, 1996; Geritz *et al.*, 1997, 1998; Dieckmann *et al.*, 2004), which can occur through all fundamental types of ecological interaction, including competition, predator–prey interaction, and mutualism (Doebeli and Dieckmann, 2000; Dieckmann *et al.*, 2007). Therefore, evolutionary branching may be an important mechanism underlying the sympatric or parapatric speciation of sexual populations driven by frequency-dependent selection pressures (e.g. Doebeli, 1996; Dieckmann and Doebeli, 1999; Kisdi and Geritz, 1999; Doebeli and Dieckmann, 2003; Dieckmann *et al.*, 2004; Claessen *et al.*, 2008; Durinx and Van Dooren, 2009; Heinz *et al.*, 2009; Payne *et al.*, 2011).

In asexual populations with rare and small mutational steps, evolutionary branching occurs through trait-substitution sequences caused by the sequential invasion of successful mutants. In univariate trait spaces, a necessary and sufficient condition for evolutionary branching is the existence of a convergence-stable trait value, called an evolutionary-branching point, at which directional selection is absent and the remaining selection is locally disruptive (Metz *et al.*, 1992; Geritz *et al.*, 1997).

Real populations, however, have undergone, and are usually undergoing, evolution in many quantitative traits, with large variation in their evolutionary speeds (e.g. Hendry and Kinnison, 1999; Kinnison and Hendry, 2001). Such speed differences among traits may be due to smaller mutation rates and/or magnitudes in some traits than in others, and will also arise when fitness is less sensitive to some traits than to others.

Only a few previous studies have analytically investigated evolutionary branching in multivariate trait spaces (Ackermann and Doebeli, 2004; Egas *et al.*, 2005; Leimar, 2005; Ravigné *et al.*, 2009). Those studies assumed that all considered traits evolve at comparable speeds, and analysed possibilities of evolutionary branching by examining the existence of evolutionary-branching points having the following four properties: evolutionary singularity (no directional selection), convergence stability (local evolutionary attractor for monomorphic evolution), evolutionary instability (locally disruptive selection), and mutual invasibility (local coexistence of dimorphic trait values). All of these studies have therefore considered the vanishing of directional selection as a prerequisite for evolutionary branching.

On the other hand, Ito and Dieckmann (2007) have numerically shown that, when mutational step sizes are not infinitesimal, evolutionary branching can occur even in directionally evolving populations, as long as directional evolution is sufficiently slow. This implies that trait spaces may contain evolutionary-branching lines that attract monomorphic evolution and then induce evolutionary branching while populations are directionally evolving along them. Furthermore, Ito and Dieckmann (submitted) derived sufficient conditions for the existence of such evolutionary-branching lines, by focusing on trait-substitution sequences formed by invasions each of which possesses maximum likelihood, called maximum-likelihood invasion paths (MLIPs).

In this study, we heuristically extend the derived sufficient conditions for evolutionary-branching lines to sufficient conditions for evolutionary-branching areas, and apply these two sets of conditions to three eco-evolutionary models with bivariate trait spaces. The paper is structured as follows. The next section explains conditions for evolutionary-branching lines and extends those to evolutionary-branching areas. In the first example, we apply the two sets of conditions to a resource-competition model with two evolving niche positions. In the second example, we show their application to another resource-competition model with evolving niche position and niche width. In the third example,

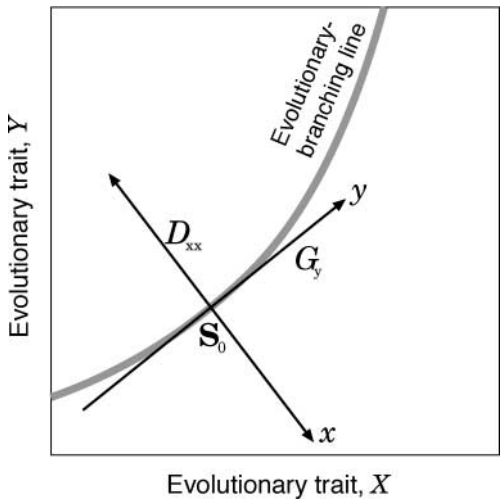

Fig. 1. Illustration of the local characteristics of an evolutionary-branching line. For checking the conditions for an evolutionary-branching line (grey line), the trait space (X, Y) (frame axes) is locally normalized so that in the new coordinates (x, y) (black lines) mutational steps are isotropic and disruptive selection is maximal in the direction of x. If at a phenotype $\mathbf{S}_0$ the maximum disruptive selection D_{xx} in the direction of x is sufficiently strong compared with the directional selection G_y in the direction of y, and if $\mathbf{S}_0$ is moreover convergence stable in the direction of x, then an evolutionary-branching line is passing through $\mathbf{S}_0$.

a predator–prey model with two evolving niche positions is analysed. The last section discusses how our conditions improve understanding of evolutionary branching in multivariate trait spaces.

CONDITIONS FOR EVOLUTIONARY-BRANCHING LINES AND AREAS

In this section, we review and explain the sufficient conditions for evolutionary-branching lines (Ito and Dieckmann, submitted) and extend them to evolutionary-branching areas. We consider bivariate trait spaces spanned by two scalar traits X and Y, denoted by $\mathbf{S} = (X, Y)^{\mathrm{T}}$ (where T denotes transposition). The conditions for evolutionary-branching lines and areas are analysed by introducing a locally normalized coordinate system $\mathbf{s} = (x, y)^{\mathrm{T}}$ at each point of the original coordinate system $\mathbf{S} = (X, Y)^{\mathrm{T}}$. Throughout this paper, all model definitions, figures, and verbal discussions of the models are presented in terms of the original coordinate systems, while the analytic conditions (e.g. in equations 1–3) are presented using the locally normalized coordinate systems.

Local normalization of invasion-fitness function

We consider an asexual monomorphic population in an arbitrary bivariate trait space $\mathbf{S} = (X, Y)^{\mathrm{T}}$. Throughout this paper, we assume low mutation rates and small mutational step sizes. Under the former assumption, the population is almost always close to population-dynamical equilibrium when a mutant emerges. It can then also be shown that, in the absence of population-dynamical bifurcations and when mutational step sizes are not only small, but infinitesimal, the population remains monomorphic in the course of

directional evolution (Geritz *et al.*, 2002): under these conditions, a mutant phenotype $\mathbf{S}'$ can invade and replace a resident phenotype $\mathbf{S}$ if its invasion fitness is positive, resulting in what is called a trait substitution.

The invasion fitness of $\mathbf{S}'$ under $\mathbf{S}$, denoted by $F(\mathbf{S}'; \mathbf{S})$, is defined as the exponential growth rate of a small population of phenotype $\mathbf{S}'$ in the environment created by a monomorphic population of phenotype $\mathbf{S}$ at its population-dynamical equilibrium (Metz *et al.*, 1992). The invasion-fitness function F can be interpreted as a fitness landscape in $\mathbf{S}'$, whose shape depends on $\mathbf{S}$. For small mutational step sizes, repeated invasion and replacement of $\mathbf{S}$ by $\mathbf{S}'$ in the direction of the fitness gradient $\partial F(\mathbf{S}'; \mathbf{S})/\partial \mathbf{S}'|_{\mathbf{S}'=\mathbf{S}}$ brings about a trait-substitution sequence, resulting in gradual directional evolution (Metz *et al.*, 1992; Dieckmann *et al.*, 1995; Dieckmann and Law, 1996; Geritz *et al.*, 2002).

When a mutant emerges, which occurs with probability μ per birth, we assume that its phenotype $\mathbf{S}'$ follows a mutation probability distribution $M(\mathbf{S}' - \mathbf{S})$ given by a bivariate normal distribution with mean $\mathbf{S}$ (see Appendix A). The distribution of mutational step sizes may depend on the direction of $\mathbf{S}' - \mathbf{S}$, according to the variance–covariance matrix of M.

In this trait space, evolutionary dynamics depend on the invasion-fitness function F and the mutation probability distribution M. To describe this dependence, we consider a monomorphic population of phenotype $\mathbf{S}_0$, and to simplify notation and analysis, we introduce a locally normalized coordinate system $\mathbf{s} = (x, y)^{\mathrm{T}}$ having its origin at $\mathbf{S}_0$ (Fig. 1). This local coordinate system is scaled so that the standard deviation of mutational step sizes, equalling the root-mean-square mutational step size, is σ in all directions. The asymmetry (non-isotropy) of mutations is thus absorbed into the invasion-fitness function, resulting in a normalized invasion-fitness function denoted by $f(\mathbf{s}'; \mathbf{s})$.

The local shape of f around the origin $\mathbf{s} = 0$ ($\mathbf{S} = \mathbf{S}_0$) can be approximated by a Taylor expansion in $\mathbf{s}$ and $\boldsymbol{\delta}\mathbf{s} = (\delta x, \delta y)^{\mathrm{T}} = \mathbf{s}' - \mathbf{s}$ up to second order,

$$f(\mathbf{s}'; \mathbf{s}) = \mathbf{G}\,\boldsymbol{\delta}\mathbf{s} + \frac{1}{2}\mathbf{s}^{\mathrm{T}}\mathbf{C}\,\boldsymbol{\delta}\mathbf{s} + \frac{1}{2}\boldsymbol{\delta}\mathbf{s}^{\mathrm{T}}\mathbf{D}\,\boldsymbol{\delta}\mathbf{s}, \tag{1}$$

with the row vector $\mathbf{G} = (G_{\mathbf{x}}, G_{\mathbf{y}})$ and the matrices $\mathbf{C} = ((C_{\mathbf{xx}}, C_{\mathbf{xy}}), (C_{\mathbf{yx}}, C_{\mathbf{yy}}))^{\mathrm{T}}$ and $\mathbf{D} = ((D_{\mathbf{xx}}, 0), (0, D_{\mathbf{yy}}))^{\mathrm{T}}$. The other possible terms in this expansion, proportional to $\mathbf{s}$ and $\mathbf{s}^{\mathrm{T}}\mathbf{s}$, vanish because $f(\mathbf{s}; \mathbf{s}) = 0$ holds at population-dynamical equilibrium for arbitrary $\mathbf{s}$. The vector $\mathbf{G} = \partial f(\mathbf{s}'; \mathbf{s})/\partial \mathbf{s}'|_{\mathbf{s}'=\mathbf{s}=\mathbf{0}}$ is the fitness gradient: it measures the steepest ascent of f with respect to $\mathbf{s}'$, and thus describes directional selection for a population at the origin. The matrix $\mathbf{C} = \partial^2 f(\mathbf{s}'; \mathbf{s})/(\partial \mathbf{s}'\partial \mathbf{s})|_{\mathbf{s}'=\mathbf{s}=\mathbf{0}}$ measures how directional selection changes as the population deviates from the origin, and thus describes evolutionary convergence to, and/or divergence from, the origin. The symmetric matrix $\mathbf{D} = \partial^2 f(\mathbf{s}'; \mathbf{s})/\partial \mathbf{s}'^2|_{\mathbf{s}'=\mathbf{s}=\mathbf{0}}$ measures the second derivative, or curvature, of f with respect to $\mathbf{s}'$, and thus describes disruptive and/or stabilizing selection at the origin. The local coordinate system $\mathbf{s} = (x, y)^{\mathrm{T}}$ can always be chosen, by adjusting the directions of the x- and y-axes, so that $\mathbf{D}$ is diagonal and $D_{\mathbf{xx}} \geq D_{\mathbf{yy}}$. Thus, when disruptive selection exists, it has maximum strength along the x-axis. Note that $\mathbf{G}$, $\mathbf{C}$, and $\mathbf{D}$ are functions of the base point $\mathbf{S}_0$.

Conditions for evolutionary-branching lines

A typical situation allowing evolutionary branching of a directionally evolving population occurs when mutational step sizes are significantly smaller in one trait direction than in

the other, when considered in the original coordinate system $\mathbf{S} = (X, Y)^{\mathrm{T}}$. In this case, the population quickly evolves in the direction of the larger step size until it no longer experiences directional selection in that direction, while it continues slow directional evolution in the other direction. Then, if the population experiences sufficiently strong disruptive selection along the fast direction compared with directional selection along the slow direction, evolutionary branching may occur.

Ito and Dieckmann (submitted) demonstrated this conclusion, by analytically deriving sufficient conditions for the existence of an evolutionary-branching line passing through $\mathbf{S_0}$ (by focusing on trait-substitution sequences formed by invasions each of which possesses maximum likelihood, so-called maximum-likelihood invasion paths or MLIPs). In the locally normalized coordinate system $\mathbf{s} = (x, y)^{\mathrm{T}}$ at $\mathbf{S_0}$, these conditions come in three parts:

$$G_{\mathbf{x}} = 0, \tag{2a}$$

$$C_{\mathbf{xx}} < 0, \tag{2b}$$

and

$$\frac{\sigma D_{\mathbf{xx}}}{|G_{\mathbf{y}}|} > \sqrt{2}. \tag{2c}$$

While equations (2) were analytically derived assuming that $C_{\mathbf{yy}}$, $C_{\mathbf{xy}}$, $C_{\mathbf{yx}}$, and $D_{\mathbf{yy}}$ are negligible, it is expected that these conditions work well even when this simplifying assumption is relaxed, as explained by Ito and Dieckmann (submitted). Equation (2a) ensures the absence of directional selection in x. Equations (2a) and (2b) ensure convergence, through directional evolution, of monomorphic populations to the evolutionary-branching line $x = 0$. After sufficient convergence, inequality (2c) ensures evolutionary branching, which according to this inequality occurs when disruptive selection $D_{\mathbf{xx}}$ orthogonal to $x = 0$ is sufficiently strong compared with directional selection $G_{\mathbf{y}}$ along $x = 0$. The smaller the standard deviation σ of mutation step sizes, the stronger disruptive selection $D_{\mathbf{xx}}$ must be relative to directional selection $G_{\mathbf{y}}$ for evolutionary branching to occur.

Note that as $|G_{\mathbf{y}}| \to 0$, inequality (2c) converges to $D_{\mathbf{xx}} > 0$, so that in this limiting case the conditions for evolutionary-branching lines in bivariate trait spaces become identical to the conditions for evolutionary-branching points in univariate trait spaces (Metz *et al.*, 1992; Geritz *et al.*, 1997). Similarly, when $\sigma \to 0$, inequality (2c) requires $G_{\mathbf{y}} = 0$ and $D_{\mathbf{xx}} > 0$, which shows that for infinitesimal mutation steps evolutionary branching can occur only in the absence of all directional selection.

By examining conditions (2) for all phenotypes $\mathbf{S_0}$ in a considered trait space, and then connecting those phenotypes that fulfil these conditions, evolutionary-branching lines are identified. According to the derivation of conditions (2), it is ensured that any MLIP starting from a monomorphic population of phenotypes sufficiently close to an evolutionary-branching line immediately converges to that line and then brings about evolutionary branching (Ito and Dieckmann, submitted). Also, trait-substitution sequences that are not MLIPs then show a very high likelihood of evolutionary branching (Ito and Dieckmann, submitted).

Conditions for evolutionary-branching areas

We now extend conditions for evolutionary-branching lines to evolutionary-branching areas. As explained below, two special cases are analytically tractable; the extended

conditions are then obtained heuristically by treating intermediate cases through interpolation.

While conditions (2) were derived as sufficient conditions for evolutionary branching, it is likely that in particular the equality condition (2a) is too strict, as evolutionary branching does not require $G_{\mathbf{x}} = 0$, but only that $|G_{\mathbf{x}}|$ be sufficiently small. But how small is small enough? To answer this question, we have to extend inequality (2c) to phenotypes that are not on an evolutionary-branching line. For such phenotypes, the orthogonality between the directions of directional selection and of maximum disruptive selection, which strictly holds on evolutionary-branching lines and is only negligibly disturbed in their immediate vicinity (Ito and Dieckmann, submitted), is increasingly relaxed the farther these phenotypes are displaced from such lines. Fortunately, the emergence of a protected dimorphism along MLIPs, which underlies inequality (2c), can be studied analytically also for the opposite case, in which the direction of directional selection is parallel to that of maximum disruptive selection (see Appendix B). By interpolating between these two special cases, we can generalize inequality (2c) to intermediate cases, in which directional selection is neither orthogonal nor parallel to disruptive selection,

$$\frac{\sigma D_{\mathbf{xx}}}{\left|\tilde{\mathbf{G}}\right|} > \sqrt{2} \text{ with } \tilde{\mathbf{G}} = (\sqrt{2}G_{\mathbf{x}},\, G_{\mathbf{y}}). \tag{3a}$$

The factor $\sqrt{2}$ in the definition of $\tilde{\mathbf{G}}$ means that directional selection in x hinders evolutionary branching in y slightly more than directional selection in y.

By combining inequalities (2b) and (3a), we obtain conditions for evolutionary-branching areas, as it is equation (2a) that limits conditions (2) to being fulfilled just along lines. Evolutionary-branching areas always surround evolutionary-branching lines when such lines exist, but also comprise phenotypes for which, in violation of equation (2a), directional evolution has not yet converged to those lines.

Since the conditions for evolutionary-branching lines and areas are derived as sufficient conditions (for the emergence of a protected dimorphism along MLIPs), the length of these lines and the size of these areas are expected to be conservative. Thus, adjusting the threshold value in equation (3a) may be useful for explaining observed patterns of evolutionary branching. For this purpose, we introduce the parameter ρ with $0 < \rho \leq 1$ into equation (3a), which gives

$$\frac{\sigma D_{\mathbf{xx}}}{\left|\tilde{\mathbf{G}}\right|} > \sqrt{2}\rho. \tag{3b}$$

Below, we illustrate the effect of ρ by considering $\rho = 0.2$. We call the combination of inequalities (2b) and (3b) the 20%-threshold condition for evolutionary-branching areas, and we refer to areas fulfilling this condition as 20%-threshold areas. For specific procedures that are useful for the practical identification of evolutionary-branching lines and areas, see Appendix C.

Sizes and shapes of evolutionary-branching lines and areas

As a simple example, we now briefly explain how an evolutionary-branching line and area are identified around an evolutionary-branching point located at the origin of a trait space $\mathbf{S} = (X,\, Y)^{\mathrm{T}}$ (see Appendix E for details).

We assume that the strengths of convergence stability of the origin along the X- and Y-axes are given by the two negative scalars $C_{\mathbf{XX}}$ and $C_{\mathbf{YY}}$, respectively. We also assume that the maximum disruptive selection in this original coordinate system occurs along the X-axis, quantified by the positive scalar $D_{\mathbf{XX}}$ (i.e. $D_{\mathbf{XX}} > D_{\mathbf{YY}}$). In addition, we denote the standard deviations of mutational step sizes along the X- and Y-axes by $\sigma_{\mathbf{X}}$ and $\sigma_{\mathbf{Y}}$, respectively. We assume that these steps have no mutational correlation, $\sigma_{\mathbf{XY}} = 0$, and that they are largest along the X-axis, $\sigma_{\mathbf{X}} > \sigma_{\mathbf{Y}}$. In this case, for each phenotype $\mathbf{S_0} = (X_0,\ Y_0)^{\mathbf{T}}$ close to the origin, local normalization provides the matrices **G**, **C**, and **D** in equation (1), without the need for any coordinate rotation, i.e. the x-axis is parallel to the X-axis.

By examining equations (2) and equation (3a) based on the derived matrices **G**, **C**, and **D**, we find, expressed in the original coordinate system, an evolutionary-branching line as a straight-line segment,

$$X_0 = 0 \qquad \text{and} \qquad |Y_0| < r_{\mathbf{Y}}, \tag{4}$$

and an evolutionary-branching area as a filled ellipse,

$$\frac{X_0^2}{r_{\mathbf{X}}^2} + \frac{Y_0^2}{r_{\mathbf{Y}}^2} < 1, \tag{5a}$$

with a radius of

$$r_{\mathbf{X}} = \frac{\sigma_{\mathbf{X}} D_{\mathbf{XX}}}{2|C_{\mathbf{XX}}|} \tag{5b}$$

along the X-axis, and a radius of

$$r_{\mathbf{Y}} = \frac{\sigma_{\mathbf{X}} D_{\mathbf{XX}}}{\sqrt{2}|C_{\mathbf{YY}}|} \cdot \frac{\sigma_{\mathbf{X}}}{\sigma_{\mathbf{Y}}} \tag{5c}$$

along the Y-axis.

Note that the length of the evolutionary-branching line coincides with the radius of the evolutionary-branching area along the Y-axis. According to equations (5), if the difference in magnitude between $\sigma_{\mathbf{X}}$ and $\sigma_{\mathbf{Y}}$ is kept small, large mutational step sizes and/or strong disruptive selection pressures result in large evolutionary-branching areas. On the other hand, according to equation (5c), when $\sigma_{\mathbf{Y}}$ is small compared with $\sigma_{\mathbf{X}}$, the shape of the evolutionary-branching area is elongated along the Y-axis, even if $\sigma_{\mathbf{X}}$ is small. Since infinitesimally small $\sigma_{\mathbf{Y}}$ make this situation identical to that of a univariate trait space comprising trait X alone, equation (5b) may work also for predicting one-dimensional evolutionary-branching areas surrounding evolutionary-branching points in univariate trait spaces.

EXAMPLE 1: RESOURCE-COMPETITION MODEL WITH EVOLVING NICHE POSITIONS

In this section, we apply our conditions for evolutionary-branching lines and areas to a model of niche evolution under intraspecific resource competition (Vukics *et al.*, 2003; Ito and Dieckmann, 2007), which is a bivariate extension of seminal models by MacArthur and Levins (MacArthur and Levins, 1967; MacArthur, 1972) and Roughgarden (1974, 1976). This example illustrates how an evolutionary-branching point transforms into an evolutionary-branching line when differences in mutational step sizes among two trait directions become sufficiently large.

Model description

We consider a bivariate trait space $\mathbf{S} = (X, Y)^{\mathrm{T}}$, with X and Y denoting evolving traits that determine a phenotype's bivariate niche position. The growth rate of phenotype $\mathbf{S}_i$ is given by

$$\frac{\mathrm{d}n_i}{\mathrm{d}t} = n_i[1 - \sum\nolimits_{j=1}^{L} \alpha(\mathbf{S}_i - \mathbf{S}_j) n_j / K(\mathbf{S}_i)], \tag{6a}$$

where L is the number of resident phenotypes. The carrying capacity $K(\mathbf{S}_i)$ of phenotype $\mathbf{S}_i$ is given by an isotropic bivariate normal distribution,

$$K(\mathbf{S}_i) = K_0 \exp(-\tfrac{1}{2} \left| \mathbf{S}_i \right|^2 / \sigma_{\mathbf{K}}^2), \tag{6b}$$

with maximum K_0, mean $(0, 0)^{\mathrm{T}}$, and standard deviation $\sigma_{\mathbf{K}}$. The strength $\alpha(\mathbf{S}_i - \mathbf{S}_j)$ of competition between phenotype $\mathbf{S}_i$ and phenotype $\mathbf{S}_j$ is also given by an isotropic bivariate normal distribution,

$$\alpha(\mathbf{S}_i - \mathbf{S}_j) = \exp(-\tfrac{1}{2} \left| \mathbf{S}_i - \mathbf{S}_j \right|^2 / \sigma_{\alpha}^2), \tag{6c}$$

with maximum 1, mean $(0, 0)^{\mathrm{T}}$, and standard deviation σ_{α}, so the strength of competition is maximal between identical phenotypes $\mathbf{S}_i = \mathbf{S}_j$ and monotonically declines with phenotypic distance $|\mathbf{S}_i - \mathbf{S}_j|$.

In this model, carrying capacity is maximal at the origin $\mathbf{S} = (0, 0)^{\mathrm{T}}$, which therefore serves as a unique convergence stable phenotype, or global evolutionary attractor, to which monomorphic populations converge through directional evolution. After sufficient convergence, if the width σ_{α} of the competition kernel is narrower than the width $\sigma_{\mathbf{K}}$ of the carrying-capacity distribution, the resultant fitness landscape has a minimum at the origin, which induces evolutionary branching of the evolving population. Thus, $\sigma_{\alpha} < \sigma_{\mathbf{K}}$ is the condition for the existence of an evolutionary-branching point in this model (Vukics *et al.*, 2003), in analogy with the univariate case (Roughgarden, 1972; Dieckmann and Doebeli, 1999).

As for the mutation probability distribution, we define its variance–covariance matrix so that the standard deviation of mutational step sizes has a maximum σ_1 in the direction of $\mathbf{e}_1 = (-1, 1)^{\mathrm{T}}$ and a minimum σ_2 in the direction of $\mathbf{e}_2 = (1, 1)^{\mathrm{T}}$.

Note that fitness in this model is rotationally symmetric in terms of the traits X and Y (i.e. rotating all phenotypes around the origin does not change their fitnesses). Thus, a sensitivity difference of the normalized invasion-fitness function can arise only from the considered difference in mutational step sizes along the two directions $\mathbf{e}_1$ and $\mathbf{e}_2$.

Predicted evolutionary-branching lines and areas

When mutational step sizes are isotropic, the predicted evolutionary-branching area forms a circle around the evolutionary-branching point, and contains no evolutionary-branching line (not shown). In this case, occurrences of evolutionary branching are explained well by the evolutionary-branching point alone. Because of the rotational symmetry in fitness, there is no restriction on the direction of evolutionary branching, so that evolutionary diversification can occur in any direction (Vukics *et al.*, 2003). Although this case is reminiscent of that of a univariate trait defined by the distance from the evolutionary-branching point,

these two cases are not equivalent: this is because in the univariate case disruptive selection and directional selection are always parallel, while in the isotropic bivariate case disruptive selection may be orthogonal to directional selection.

Figure 2a shows that when the difference in mutational step size between directions $\mathbf{e}_1$ and $\mathbf{e}_2$ is substantial (e.g. $\sigma_1/\sigma_2 = 3$), the evolutionary-branching line and area expand in the direction of the smaller mutational step size ($\mathbf{e}_2$ in this case). In addition, the direction of expected evolutionary diversification becomes more restricted to $\mathbf{e}_1$ the larger this difference becomes. [If $\mathbf{e}_1$ and $\mathbf{e}_2$ were pointing along the Y- and X-axis, respectively, the situation would correspond to equations (4) and (5).] In Fig. 2a, the short purple line and the small purple area (both situated within the light-purple area) depict the predicted evolutionary-branching line and area, with their colours indicating the predicted direction of diversification. Because of the difference in mutational step sizes between the two directions, it is expected that a monomorphic population quickly converges to the line $Y = X$ (grey arrows) and then slowly converges to the evolutionary-branching area. Evolutionary branching is expected to occur at the latest once evolution has reached this area, because our conditions for an evolutionary-branching area are derived as sufficient conditions and imply the possibility of an immediate start of evolutionary branching of a monomorphic population in its inside. Accordingly, evolutionary branching may occur well before the population has reached the evolutionary-branching area. The light-purple area shows the corresponding 20%-threshold area, comprising all phenotypes that fulfil the 20%-threshold condition for evolutionary-branching areas. By definition, an evolutionary-branching area is always included in the corresponding 20%-threshold area. The larger the difference in mutational step sizes between the two directions, the longer the evolutionary-branching line and the more elongated the evolutionary-branching area, as predicted by equation (5c).

Comparison with actual evolutionary dynamics

Figure 2b shows occurrences of evolutionary branching in numerically calculated evolutionary dynamics starting from monomorphic populations with phenotypes randomly chosen across the shown trait space: each occurrence is depicted by an open triangle whose colour indicates the direction of that particular evolutionary branching. The evolutionary dynamics are numerically calculated as trait-substitution sequences according to the oligomorphic stochastic model of adaptive dynamics theory (Ito and Dieckmann, 2007) (for the sake of computational efficiency, phenotypes with densities below a threshold ε_e are removed, with the value of ε_e being immaterial as long as it is small enough). The relative shape of the cluster of occurrences is characterized well by the evolutionary-branching area, or here almost equivalently, by the evolutionary-branching line. Moreover, the absolute shape, and hence the size, of this cluster is well matched by that of the 20%-threshold area. The fact that the colour of the triangles in Fig. 2b is very similar to that of the evolutionary-branching area in Fig. 2a also demonstrates that the predicted and actual directions of diversification are in good agreement.

Figure 2b shows two evolutionary trajectories, depicted as dark-yellow and green curves, respectively. These illustrate that monomorphic populations initially converge to the line $Y = X$. Then, if the population is already inside the evolutionary-branching area, it immediately undergoes evolutionary branching, as expected (green curves in Fig. 2b and Fig. 2d). In contrast, if the population still remains outside the evolutionary-branching

area, it continues directional evolution along the line $Y = X$ towards the evolutionary-branching area. As expected, evolutionary branching may occur before the population has reached the evolutionary-branching area (dark-yellow curves in Fig. 2b and Fig. 2c).

In summary, this first example shows how differences in mutational step sizes among trait directions can transform an evolutionary-branching point into an evolutionary-branching line or an elongated evolutionary-branching area.

EXAMPLE 2: RESOURCE-COMPETITION MODEL WITH EVOLVING NICHE POSITION AND NICHE WIDTH

In this section, based on another type of resource-competition model, we show that an evolutionary-branching area can exist without containing any evolutionary-branching point.

Model description

For phenotypes $\mathbf{S} = (X, Y)^{\mathrm{T}}$ in our second example, the trait X still determines the phenotype's niche position, as in the first model, whereas the trait Y now determines the phenotype's niche width, differently from the first model. This niche width can be interpreted in terms of the variety of resource types utilized by the phenotype. We assume a constant and unimodal distribution $R(z)$ of univariate resource types z, given by a normal distribution,

$$R(z) = R_0 \mathrm{N}(z, m_{\mathbf{R}}, \sigma_{\mathbf{R}}^2), \tag{7a}$$

with $\mathrm{N}(z, m, \sigma^2) = \exp(-\frac{1}{2}(z-m)^2/\sigma^2)/(\sqrt{2\pi}\sigma)$. Here, R_0, $m_{\mathbf{R}}$, and $\sigma_{\mathbf{R}}$ denote the resource distribution's integral, mean, and standard deviation respectively. Similarly, the niche of a phenotype $\mathbf{S}_i$ is specified by a normal distribution across resource types z, with mean X_i (niche position) and standard deviation Y_i (niche width),

$$c(z, \mathbf{S}_i) = \mathrm{N}(z, X_i, Y_i^2). \tag{7b}$$

The rate of potential resource gain of phenotype $\mathbf{S}_i$ per unit of its biomass is given by the overlap integral, over all resource types z, of its niche $c(z, \mathbf{S}_i)$ and the resource distribution $R(z)$. The corresponding rate of actual resource gain $g(\mathbf{S}_i)$ incorporates a functional response, derived in Appendix D as an extension of the Beddington-DeAngelis-type functional response (Beddington, 1975; DeAngelis *et al.*, 1975), known to ensure both saturation of consumption and interference competition among consumers. On this basis, the growth rate of phenotype $\mathbf{S}_i$ is given by

$$\frac{\mathrm{d}n_i}{\mathrm{d}t} = n_i[\lambda g(\mathbf{S}_i) - d(Y_i)], \tag{7c}$$

where the constant λ measures trophic efficiency (i.e. biomass production per biomass gain) and $d(Y_i)$ is the biomass loss of phenotype $\mathbf{S}_i$ due to basic metabolism and natural death, with the dependence on Y_i reflecting costs of specialization or generalization.

As for the mutation distribution, we use a simple bivariate normal distribution in which the standard deviation of mutational step sizes has its maximum $\sigma_{\mathbf{X}}$ in the X-direction and its minimum $\sigma_{\mathbf{Y}}$ in the Y-direction. See Appendix E for further model details.

Predicted evolutionary-branching lines and areas

Figure 3a shows the directional evolution (grey arrows) of monomorphic populations and the predicted evolutionary-branching lines and areas, as in Fig. 2a, for the case that specialization (narrow niche width) is costly. This shows that niche position and niche width directionally evolve so as to become more similar, respectively, to the centre and width of the resource distribution. We find two kinds of evolutionary-branching areas. As indicated by the colour coding, the small blue evolutionary-branching area around the centre of the shown trait space induces evolutionary branching in the direction of niche width. This evolutionary-branching area contains an evolutionary-branching point at its centre and attracts any monomorphic population in the trait space. In this regard, this evolutionary-branching area is similar to that in our first model. In contrast, the red evolutionary-branching area around the bottom of the shown trait space contains no evolutionary-branching point, although it does contain an evolutionary-branching line along $X = 0.5$. Moreover, as indicated by the colour coding, this evolutionary-branching line and area induce evolutionary branching in the direction of niche position. It is therefore clear that the two identified evolutionary-branching areas are qualitatively different from each other.

Comparison with actual evolutionary dynamics

Figure 3b shows occurrences of evolutionary branching in numerically calculated evolutionary dynamics, as in Fig. 2b. There exist three clusters: a blue one around the centre, a small red one around $\mathbf{S} = (0.5, 0.16)^{\mathrm{T}}$, and a large red one along the bottom of the shown trait space. Except for the small red cluster, the shapes of these clusters coincide well with the two identified evolutionary-branching areas. Also, as shown by the colour coding, the directions of observed diversifications are predicted well by those areas.

As for the blue evolutionary-branching area, the observed process of evolutionary branching in niche width (dark-yellow curves in Fig. 3b) is always slow, as shown in Fig. 3c. In contrast, the large red evolutionary-branching area induces fast and repeated evolutionary branching in niche position (green curves in Fig. 3b), generating four lineages at the end of the time window in Fig. 3d. The timescale difference between these two types of branching dynamics exceeds a factor of 100.

This difference in evolutionary speed can be explained as follows. When a population comes close to the blue evolutionary-branching area, the shape of its niche is similar to the resource distribution, resulting in weak selection pressures, including disruptive selection. In this case, the process of evolutionary branching is therefore expected to be slow. On the other hand, when a population is close to, or located inside, the red evolutionary-branching area, its niche is much narrower than the resource distribution. This situation creates strong disruptive selection in niche position. In this case, the process of evolutionary branching is thus expected to proceed rapidly.

This second example shows that our conditions for evolutionary-branching areas can identify such areas containing no evolutionary-branching point. Here, such an area induces a qualitatively different mode of evolutionary branching than the existing evolutionary-branching area that contains an evolutionary-branching point. Note, however, that our conditions for evolutionary-branching areas do not explain the separation between the small and large red clusters in Fig. 3b. In addition, the size of the blue cluster in Fig. 3b is much larger than that of the corresponding 20%-threshold area in Fig. 3a, which is not explained either.

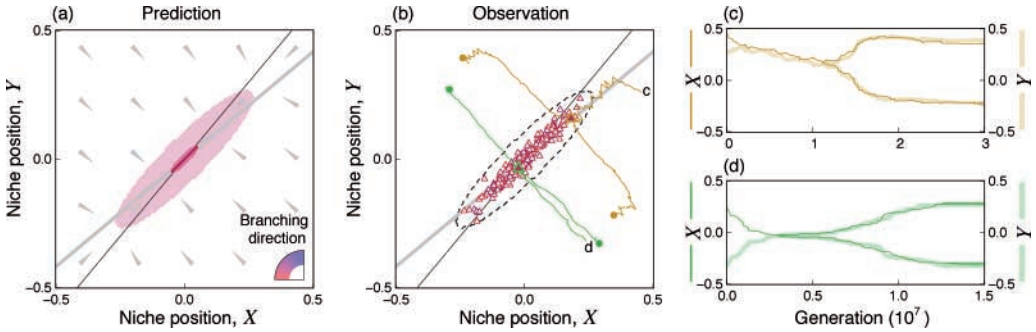

Fig. 2.

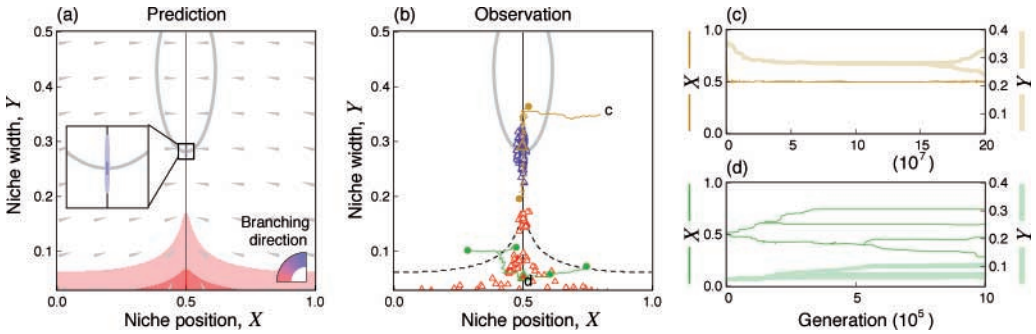

Fig. 3.

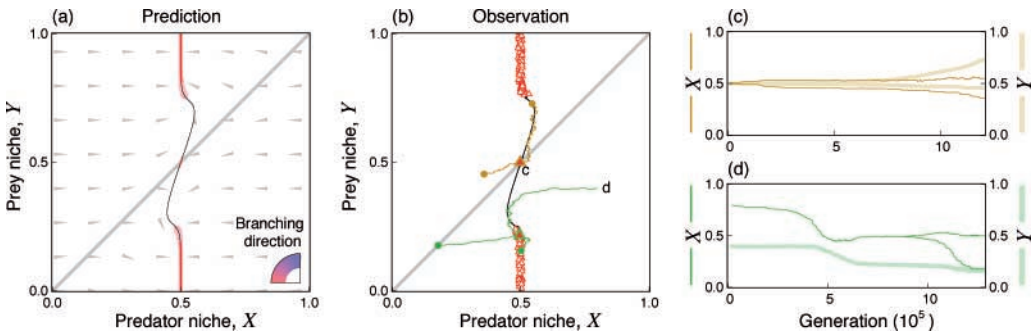

Fig. 4.

EXAMPLE 3: PREDATOR–PREY MODEL WITH EVOLVING NICHE POSITIONS

In this section, based on a predator–prey model, we show that evolutionary branching can occur even if a model's entire trait space contains no evolutionary-branching point, so that any occurrence of evolutionary branching is explained by evolutionary-branching lines and areas.

Fig. 2. Prediction and observation of evolutionary-branching lines and areas in a resource-competition model with evolving bivariate niche positions and non-isotropic mutational steps. (a) Predicted evolutionary-branching line, evolutionary-branching area, and 20%-threshold area, depicted by a line segment and by two nested areas filled with dark and light colours, respectively. The colours of the line and areas follow a red–blue gradation indicating the predicted directions of evolutionary branching: pure red and pure blue correspond to evolutionary branching in the directions of the X-axis and Y-axis, respectively. Grey arrows indicate the directional evolution of monomorphic populations. The black and grey lines are zero-isoclines of the fitness gradient in the directions of the traits X and Y, respectively. (b) Occurrences of evolutionary branching (triangles) in numerically calculated evolutionary dynamics starting from 200 phenotypes randomly chosen from a uniform distribution across the shown trait space. The same colours as in (a) are used to indicate the observed directions of evolutionary branching. To facilitate comparison, the dashed curve repeats the boundary of the 20%-threshold area from (a). Two example trajectories of evolutionary dynamics are shown as dark-yellow and green curves, respectively, with initial phenotypes marked by the letters 'c' and 'd.' These marks match the panels on the right, showing evolutionary dynamics over time, with thick and thin curves corresponding to the traits X and Y, respectively. Solid circles in (b) indicate the final phenotypes shown in (c) and (d), while solid triangles in (b) indicate the phenotypes at which evolutionary branching occurs in the two example trajectories. Parameters: $\sigma_{\mathbf{K}} = 0.8$, $\sigma_{\alpha} = 0.5$, $K_0 = 1000$, $\varepsilon_{\mathbf{e}} = 10^{-5}$, $\mu = 10^{-5}$, $\sigma_1 = 0.01$, $\sigma_2 = 0.003$.

Fig. 3. Prediction and observation of evolutionary-branching lines and areas in a resource-competition model with evolving niche positions and widths. (a) Predicted evolutionary-branching line (red line at the centre bottom), evolutionary-branching areas (red and small blue areas), and 20%-threshold areas (light-red and light-blue areas). Other elements are as in Fig. 2a. The inset shows a magnified view of the evolutionary-branching areas and corresponding 20%-threshold area around the evolutionary-branching point at $(X, Y) = (0, 0.282)$. (b) Occurrences of evolutionary branching (triangles) in numerically calculated evolutionary dynamics starting from 700 phenotypes randomly chosen from a uniform distribution across the shown trait space. Two example trajectories of evolutionary dynamics are shown as in Fig. 2b. Other elements are as in Fig. 2b. Parameters: $\sigma_{\mathbf{R}} = 0.2$, $m_{\mathbf{R}} = 60$, $R_0 = 400$, $\lambda = 0.3$, $\alpha = \beta = \gamma = 1$, $d_0 = 0.1$, $d_1 = 0.5$, $\varepsilon_{\mathbf{e}} = 10^{-5}$, $\mu = 10^{-5}$, $\sigma_{\mathbf{X}} = 0.01$, $\sigma_{\mathbf{Y}} = 0.003$ (α, β, and γ are introduced in Appendix D, while d_0 and d_1 are introduced in Appendix E).

Fig. 4. Prediction and observation of evolutionary-branching lines and areas in a predator–prey model with evolving predator-niche and prey-niche positions. (a) Predicted evolutionary-branching lines (red lines), evolutionary-branching areas (red areas), and 20%-threshold areas (light-red areas). Other elements are as in Figs. 2a and 3a. (b) Occurrences of evolutionary branching (triangles) in numerically calculated evolutionary dynamics starting from 200 phenotypes randomly chosen from a uniform distribution across the shown trait space. Two example trajectories of evolutionary dynamics are shown as in Figs. 2b and 3b. Other elements are as in Figs. 2b and 3b. Parameters: $\sigma_{\mathbf{c}} = \sigma_{\mathbf{r}} = 0.06$, $\sigma_{\mathbf{R}} = 0.08$, $R_0 = 4000$, $m_{\mathbf{R}} = 60$, $\lambda = 0.3$, $\alpha = 5$, $\beta = \gamma = 1$, $d = 0.1$, $\varepsilon_{\mathbf{e}} = 10^{-5}$, $\mu = 10^{-5}$, $\sigma_{\mathbf{X}} = 0.003$, $\sigma_{\mathbf{Y}} = 0.001$ (α, β, and γ are introduced in Appendix D).

Model description

The third model is a modification of the second model towards predator–prey interactions, and was developed by Ito *et al.* (2009) (see Appendix F for details). As in the first and second models, trait X still determines a phenotype's niche position. Now, however, trait Y is not a niche width as in the second model, but describes the niche position at which the corresponding phenotype can be consumed as a resource, and is therefore potentially preyed upon by other phenotypes. We thus refer to X and Y as predator-niche position and prey-niche position, respectively. Accordingly, phenotype $\mathbf{S}_i$ exists not only as a consumer (predator) with niche

$$c(z, \mathbf{S}_i) = \mathrm{N}(z, X_i, \sigma_\mathrm{c}^2), \tag{8a}$$

but also provides a resource (prey) distribution for predators, with each of its biomass units contributing according to

$$r(z, \mathbf{S}_i) = \mathrm{N}(z, Y_i, \sigma_\mathrm{r}^2), \tag{8b}$$

where the widths of these two distributions are constant and given by σ_c and σ_r, respectively. The basal-resource distribution $B(z) = R_\mathbf{0}\mathrm{N}(z, m_\mathbf{R}, \sigma_\mathbf{R}^2)$, with integral $R_\mathbf{0}$, mean $m_\mathbf{R}$, and standard deviation $\sigma_\mathbf{R}$, is analogous to the resource distribution in equation (7a) for the second model. In analogy with the second model, the rates of resource gain and biomass loss of phenotype $\mathbf{S}_i$, denoted by $g(\mathbf{S}_i)$ and $l(\mathbf{S}_i)$, respectively, are obtained as overlap integrals of niches and existing resources. Consequently, the growth rate of phenotype $\mathbf{S}_i$ is given by

$$\frac{\mathrm{d}n_i}{\mathrm{d}t} = n_i[\lambda g(\mathbf{S}_i) - l(\mathbf{S}_i) - d], \tag{8c}$$

where the rate d of biomass loss by metabolism and natural death is now assumed to be constant, differently from the second model. As in the second model, we use a simple bivariate normal mutation distribution in which the standard deviation of mutational step sizes has its maximum $\sigma_\mathbf{X}$ in the X-direction and its minimum $\sigma_\mathbf{Y}$ in the Y-direction.

Predicted evolutionary-branching lines and areas

Figure 4a shows the directional evolution (grey arrows) and predicted evolutionary-branching lines and areas, as in Fig. 2a and Fig. 3a. This shows that monomorphic populations directionally evolve so that their prey-niche positions become more distant from their predator-niche positions, while their predator-niche positions become closer to their prey-niche positions and/or the mean of the basal-resource distribution (Ito *et al.*, 2009).

A unique evolutionarily singular point at $\mathbf{S} = (0.5, 0.5)^\mathrm{T}$ matches the centre of the basal-resource distribution at $z = m_\mathbf{R} = 0.5$. This corresponds to a cannibalistic population exploiting both the basal resource and itself. As the basal-resource distribution is assumed to be wider than the predator niche, $\sigma_\mathbf{R} > \sigma_\mathrm{c}$, disruptive selection along X is expected, similarly to the first example. However, the zero-isocline of the fitness gradient in the Y-direction (thick grey curve in Fig. 4a) repels monomorphic populations in the Y-direction, although the corresponding zero-isocline in the X-direction (thin black curve) attracts them in the X-direction. Therefore, depending on the relative mutation probabilities and mutational step sizes in X and Y, the evolutionarily singular point at the intersection of

those two zero-isoclines may not be convergence stable (Dieckmann and Law, 1996; Leimar, 2009) [for analogous results for multi-locus genetics, see Mattessi and Di Pasquale (1996)], in which case there is no evolutionary-branching point in this trait space.

According to our conditions for evolutionary-branching lines, evolutionary branching by disruptive selection in X may occur when a phenotype's prey-niche position becomes sufficiently distant from its predator-niche position, so that directional selection on the prey-niche position becomes sufficiently weak. And as expected, there exist evolutionary-branching lines along the evolutionary zero-isocline for X (red line segments). Evolutionary-branching areas also exist, but are very thin; only the 20%-threshold areas are sufficiently large to become visible in Fig. 4a (light-red areas). As shown by the colour coding for evolutionary-branching lines and areas, evolutionary branching is solely expected in the direction of the predator-niche position.

There also exists a very small evolutionary-branching area around the evolutionarily singular point at the centre, which, however, may induce evolutionary branching only when the initial phenotype is located within this area, as this singular point is lacking convergence stability.

Comparison with actual evolutionary dynamics

Figure 4b shows occurrences of evolutionary branching in numerically calculated evolutionary dynamics, as in Fig. 2b and Fig. 3b. The shapes of the clusters, as well as the directions of observed evolutionary branching, are predicted well by the evolutionary-branching lines and areas. Also, the sizes of these clusters are predicted well by the 20%-threshold areas.

As shown in Fig. 4b (green curves) and Fig. 4d, a monomorphic population first converges to the evolutionary zero-isocline for X (thin black curve), and then brings about evolutionary branching when it has come sufficiently close to one of the evolutionary-branching lines.

Also, as predicted, evolutionary branching in the small evolutionary-branching area at the centre is possible, provided the initial phenotype is located within this area (dark-yellow curves in Fig. 4b and Fig. 4c). However, since this evolutionary-branching area is very small and does not contain an evolutionary attractor, almost all observed diversifications are induced by the identified evolutionary-branching lines.

Even when the predator niche is wider than the prey niche and the basal-resource distribution ($\sigma_c > \sigma_r, \sigma_R$; e.g. when $\sigma_c = 0.081$ slightly exceeds $\sigma_r = \sigma_R = 0.08$, while $\sigma_X = 0.003$ and $\sigma_Y = 0.0003$), evolutionary-branching lines can exist and induce diversification (not shown). In any case, the initial evolutionary branching always occurs adjacent to the evolutionary-branching lines.

Interestingly, evolutionary branching in this model can be recurrent: this may result in complex food webs of coexisting phenotypes, including the evolutionarily stable emergence of multiple trophic levels (Ito *et al.*, 2009).

DISCUSSION

In this paper, we have presented conditions for evolutionary-branching lines and areas, and have explored their utility by numerically analysing evolutionary branching in three different eco-evolutionary models defined with bivariate trait spaces. The first model,

a resource-competition model with evolving niche positions, has shown how an evolutionary-branching point transforms into an evolutionary-branching line and elongated evolutionary-branching area, due to differences in mutational step sizes among the two trait directions. The second model, a resource-competition model with evolving niche position and niche width, has shown the existence of an evolutionary-branching line and area containing no evolutionary-branching point, which induce a qualitatively different mode of evolutionary branching than the also existing evolutionary-branching point. The third model, a predator–prey model with evolving predator- and prey-niche positions, has shown that even when a model's entire trait space contains no evolutionary-branching point, evolutionary branching may still be bound to occur along evolutionary-branching lines and within evolutionary-branching areas. Below we discuss these phenomena in greater detail.

To understand the transformation of an evolutionary-branching point into an evolutionary-branching line and an elongated evolutionary-branching area in the first model, it is helpful to recognize that an evolutionary-branching line becomes straight and infinitely long in the limit of mutational step sizes parallel to that line converging to 0. In this limit, the resultant evolutionary dynamics are effectively univariate and occur vertically to the evolutionary-branching line. In the resultant effectively univariate trait space, the evolutionary-branching line then corresponds to an evolutionary-branching point. Thus, the curvatures and finite lengths of evolutionary-branching lines can be appreciated as resulting from eco-evolutionary settings that are intermediate between the two extremes of effectively univariate trait spaces (Metz *et al.*, 1992; Geritz *et al.*, 1997) and fully bivariate ones (Vukics *et al.*, 2003; Ackermann and Doebeli, 2004; Egas *et al.*, 2005; Ito and Dieckmann, 2007).

In our examples, such settings are created by considering different mutational step sizes in two directions of trait space. Importantly, the very same effects also arise when invasion-fitness functions possess different sensitivities to trait changes in two directions of trait space. This is simply because such sensitivity differences can be translated into differences in mutational step sizes by suitably rescaling trait space. In many settings, these two types of differences are formally indistinguishable, and are jointly captured by the local normalization of trait space we have described. The situation is different when the traits contributing to a multivariate phenotype happen to be defined on the same, or naturally comparable, scales. In such special settings, it is possible to assess whether the emergence of evolutionary-branching lines and areas is due to differences in mutational steps, differences in fitness sensitivities, or a combination thereof.

The existence of evolutionary-branching lines and areas containing no evolutionary-branching points, observed in our second and third examples, will go unnoticed by any analysis restricted to identifying evolutionary-branching points. Extending past and future theoretical studies by accounting for our conditions for evolutionary-branching lines and areas is therefore advisable, as modes of evolutionary diversification in the underlying models may otherwise be missed.

For instance, our conditions have revealed that if disruptive selection is particularly strong, evolutionary branching can occur even in the face of considerable directional selection. This mode is characterized by a rapid progression of the diversification, as illustrated by our second example when a population's niche is much narrower than the resource distribution (Fig. 3d). In this situation, evolutionary branching in niche position is rapidly repeated, accompanied by gradual evolutionary generalization. Consequently, such evolutionary dynamics are expected to occur also in models examined in previous studies of the joint evolution of niche position and niche width (Ackermann and Doebeli, 2004;

Egas *et al*., 2005; Ito and Shimada, 2007). Accordingly, this finding could open up new perspectives for understanding empirically observed instances of adaptive radiation, such as in Darwin's finches (Grant and Grant, 2008), cichlid fish (Seehausen, 2006), sticklebacks (Bell and Foster, 1994; Schluter, 2000), and anolis lizards (Losos, 2009).

Our third model, a predator–prey model with evolving niche positions, illustrates how it is straightforward to draw qualitative conclusions from our conditions for evolutionary-branching lines and areas. Specifically, when the width of the predator niche is similar to that of the basal-resource distribution, there can be no particularly strong disruptive selection. Therefore, directional selection vertical to the disruptive selection needs to be sufficiently weak if evolutionary branching is to occur. This is possible only when a phenotype's prey-niche position is distant from its predator-niche position, giving rise to the evolutionary-branching lines and areas shown in Fig. 4a. Applying our conditions, analogous evolutionary-branching lines and areas can be identified also in other predator–prey models (Ito and Ikegami, 2006; Ito *et al.*, 2009) that are comparable to our third model (not shown).

In a similar vein, we can consider predator–prey models that differ from our third model. For example, in the predator–prey model of Brännström *et al.* (2011), the predator-niche and prey-niche positions are given by a single trait, resulting in a univariate trait space that has a single evolutionary-branching point. While univariate trait spaces naturally cannot contain evolutionary-branching lines or areas, our findings here suggest that it will be interesting to extend the model of Brännström *et al.* (2011) so that the predator-niche and prey-niche positions can evolve separately: the previously found evolutionary-branching point is then expected to transform into evolutionary-branching lines and areas, and additional evolutionary-branching lines and areas containing no evolutionary-branching point might emerge.

It may also be worthwhile to revisit, in light of our conditions, a study by Doebeli and Dieckmann (2000) that also demonstrated evolutionary branching driven by predator–prey interactions. Their model considered two univariate traits, one for a predator's predator-niche position and one for a prey's prey-niche position: thus, the predator can adapt only in terms of its predator-niche position, while the prey can adapt only in terms of its prey-niche position. Although this doubly univariate setting formally differs from the bivariate setting we have analysed in the present study, applying our conditions might help reveal the existence of evolutionary-branching lines and areas in the model by Doebeli and Dieckmann (2000).

Our conditions for evolutionary-branching lines and areas are analytically derived from assessing the potential for immediate evolutionary branching of a monomorphic population (Ito and Dieckmann, submitted). Since these conditions are sufficient, but not necessary, evolutionary branching in numerically calculated evolutionary dynamics may occur under a wider range of conditions, reflecting the gradual integration of local probabilistic rates of evolutionary branching along monomorphic evolutionary trajectories. Accordingly, no full agreement between these two perspectives can be expected. It is therefore encouraging that the results presented here have demonstrated that the positions and shapes of clusters of occurrences of evolutionary branching are well predicted by evolutionary-branching areas. Moreover, the sizes of those clusters are well predicted by the corresponding 20%-threshold areas in many, but not all, cases (see, for example, the small blue evolutionary-branching area in Fig. 3a). A further potential cause of disparity is that our conditions for evolutionary-branching areas use only partial information about the local

selection pressures, assuming that the second-order derivatives C_{yy}, C_{xy}, C_{yx}, and D_{yy} (as measured in the locally normalized coordinate systems) are not important. Occasionally, these additional characteristics of the local shapes of fitness landscapes might well affect the local probabilistic rates of evolutionary branching. A formal analysis of these effects, if it turned out to be technically feasible, might improve predictive of performance.

Our results in this study are based on restrictive assumptions, such as small mutation rates, large population sizes, bivariate normal mutation distributions, and asexual reproduction. It is therefore desirable to examine the robustness of our results by relaxing or varying those assumptions. First, when mutation rate is large, evolutionary dynamics are no longer described by trait-substitution sequences, but instead amount to gradual changes of polymorphic trait distributions. In this case, one could attempt to define an effective mutation probability distribution by considering the convolution of the phenotype distribution with the actual mutation probability distribution. As this convolution is always wider than the actual mutation probability distribution alone, and as the conditions for evolutionary-branching lines and areas predict higher likelihoods of evolutionary branching for larger mutational step sizes, large mutation rates may effectively increase those likelihoods. Second, when population sizes are not sufficiently large, demographic stochasticity may destroy protected dimorphisms shortly after their emergence, as the two coexisting phenotypes initially are almost ecologically neutral (Claessen *et al.*, 2007, 2008). This can suppress evolutionary branching. Third, variations of the mutation probability distribution, keeping its variance–covariance matrix constant, may enhance or suppress the likelihood of evolutionary branching, depending on the specific shapes considered. Fourth, sexual reproduction is expected to suppress evolutionary branching, as the continuous production of intermediate offspring phenotypes counteracts diversification by disruptive selection (Dieckmann and Doebeli, 1999; Kisdi and Geritz, 1999).

As for mutation rates and mutation probability distributions, Ito and Dieckmann (submitted) have already shown that (for C_{yy}, C_{xy}, C_{yx}, $D_{yy} = 0$ in the normalized coordinate systems) the derived conditions for evolutionary-branching lines are reasonably robust to making mutation rates larger and letting mutation distributions deviate from being normal. This robustness may nevertheless be affected by making population sizes smaller than those already analysed, so that demographic stochasticity becomes relatively more important. As for sexual reproduction, Ito and Dieckmann (2007) have demonstrated numerically the evolutionary branching of sexual populations induced by evolutionary-branching lines. This previous work considered the joint evolution of several quantitative traits, an ecological trait and mating traits, with additive multi-locus genetics, free recombination, and not-small mutation rates. This analysis has demonstrated that when the evolution of assortative mating is difficult, evolutionary branching will often be suppressed, which implies that sexual reproduction may cause the likelihood of evolutionary branching to be overestimated by the conditions reported here for evolutionary-branching lines and areas in asexual populations.

Although we have focused on bivariate trait spaces in this study (to facilitate visual inspection), the conditions for evolutionary-branching lines derived by Ito and Dieckmann (submitted) readily apply to multivariate trait spaces, and our conditions for evolutionary-branching areas generalize analogously. Moreover, our conditions for evolutionary-branching lines and areas are expected to be applicable also to co-evolutionary dynamics and to the dynamics of subsequent evolutionary branching after a primary evolutionary branching has occurred. From a computational perspective, it is promising to interleave

the application of our conditions with the time integration of the canonical equation of adaptive dynamics theory (Dieckmann and Law, 1996): in this way, the deterministic approximation of evolutionary branching provided by our conditions can be integrated with the deterministic approximation of directional evolutionary and co-evolutionary dynamics provided by the canonical equation, resulting in a deterministic oligomorphic model of phenotypic evolution.

In conclusion, our conditions for evolutionary-branching lines and areas have yielded two new insights into evolutionary branching. First, evolutionary-branching points can transform into evolutionary-branching lines and areas, due to differences in mutational steps and/or fitness sensitivities among directions in trait spaces. Second, evolutionary-branching lines and areas can exist independently of evolutionary-branching points, which allows diversification even when an entire trait space contains not a single evolutionary-branching point.

ACKNOWLEDGEMENTS

The authors thank the organizers, participants, and sponsors of the workshop on Niche Theory and Speciation, which took place in Keszthely, Hungary, in August 2011, and provided the platform for developing the special issue for which this article has been prepared. The workshop was organized under the auspices of the European Research Networking Programme on Frontiers of Speciation Research (FroSpects), funded by the European Science Foundation. U.D. gratefully acknowledges financial support by the European Science Foundation, the Austrian Science Fund, the Austrian Ministry of Science and Research, and the Vienna Science and Technology Fund, as well as by the European Commission, through the Marie Curie Research Training Network FishACE and the Specific Targeted Research Project FinE.

REFERENCES

Ackermann, M. and Doebeli, M. 2004. Evolution of niche width and adaptive diversification. *Evolution*, **58**: 2599–2612.

Beddington, J.R. 1975. Mutual interference between parasites or predators and its effect on searching efficiency. *J. Anim. Ecol.*, **44**: 331–340.

Bell, M.A. and Foster, S.A. 1994. *The Evolutionary Biology of the Threespine Stickleback*. Oxford: Oxford University Press.

Brännström, Å., Loeuille, N., Loreau, M. and Dieckmann, U. 2011. Emergence and maintenance of biodiversity in an evolutionary food-web model. *Theor. Ecol.*, **4**: 467–478.

Claessen, D., Andersson, J., Persson, L. and de Roos, A.M. 2007. Delayed evolutionary branching in small populations. *Evol. Ecol. Res.*, **9**: 51–69.

Claessen, D., Andersson, J. and Persson, L. 2008. The effect of population size and recombination on delayed evolution of polymorphism and speciation in sexual populations. *Am. Nat.*, **172**: E18–E34.

DeAngelis, D.L., Goldstein, R.A. and O'Neill, R.V. 1975. A model for tropic interaction. *Ecology*, **56**: 881–892.

Dieckmann, U. and Doebeli, M. 1999. On the origin of species by sympatric speciation. *Nature*, **400**: 354–357.

Dieckmann, U. and Law, R. 1996. The dynamical theory of coevolution: a derivation from stochastic ecological processes. *J. Math. Biol.*, **34**: 579–612.

Dieckmann, U., Marrow, P. and Law, R. 1995. Evolutionary cycling in predator–prey interactions: population dynamics and the Red Queen. *J. Theor. Biol.*, **176**: 91–102.

Dieckmann, U., Doebeli, M., Metz, J.A.J. and Tautz, D. eds. 2004. *Adaptive Speciation*. Cambridge: Cambridge University Press.

Dieckmann, U., Brännström, Å., HilleRisLambers, R. and Ito, H.C. 2007. The adaptive dynamics of community structure. In *Mathematics for Ecology and Environmental Sciences* (Y. Takeuchi, K. Sato and Y. Iwasa, eds.), pp. 145–177. Berlin: Springer-Verlag.

Doebeli, M. 1996. A quantitative genetic model for sympatric speciation. *J. Evol. Biol.*, **9**: 893–909.

Doebeli, M. and Dieckmann, U. 2000. Evolutionary branching and sympatric speciation caused by different types of ecological interactions. *Am. Nat.*, **156**: S77–S101.

Doebeli, M. and Dieckmann, U. 2003. Speciation along environmental gradients. *Nature*, **421**: 259–264.

Durinx, M. and Van Dooren, T.J. 2009. Assortative mate choice and dominance modification: alternative ways of removing heterozygote disadvantage. *Evolution*, **63**: 334–352.

Egas, M., Sabelis, M.W. and Dieckmann, U. 2005. Evolution of specialization and ecological character displacement of herbivores along a gradient of plant quality. *Evolution*, **59**: 507–520.

Geritz, S.A.H., Metz, J.A.J., Kisdi, É. and Meszéna, G. 1997. Dynamics of adaptation and evolutionary branching. *Phys. Rev. Lett.*, **78**: 2024–2027.

Geritz, S.A.H., Kisdi, É., Meszéna, G. and Metz, J.A.J. 1998. Evolutionarily singular strategies and the adaptive growth and branching of the evolutionary tree. *Evol. Ecol.*, **12**: 35–57.

Geritz, S.A.H., Gyllenberg, M., Jacobs, F.J.A. and Parvinen, K. 2002. Invasion dynamics and attractor inheritance. *J. Math. Biol.*, **44**: 548–560.

Grant, B.R. and Grant, P. 2008. *How and Why Species Multiply: The Radiation of Darwin's Finches*. Princeton: Princeton University Press.

Heinz, S.K., Mazzucco, R. and Dieckmann, U. 2009. Speciation and the evolution of dispersal along environmental gradients. *Evol. Ecol.*, **23**: 53–70.

Hendry, A.P. and Kinnison, M.T. 1999. The pace of modern life: measuring rates of contemporary microevolution. *Evolution*, **53**: 1637–1653.

Ito, H.C. and Dieckmann, U. 2007. A new mechanism for recurrent adaptive radiations. *Am. Nat.*, **170**: E96–E111.

Ito, H.C. and Dieckmann, U. (submitted). Evolutionary branching under slow directional evolution.

Ito, H.C. and Ikegami, T. 2006. Food web formation through recursive evolutionary branching. *J. Theor. Biol.*, **238**: 1–10.

Ito, H.C. and Shimada, M. 2007. Niche expansion: coupled evolutionary branching of niche position and width. *Evol. Ecol. Res.*, **9**: 675–695.

Ito, H.C., Shimada, M. and Ikegami, T. 2009. Coevolutionary dynamics of adaptive radiation for food-web development. *Popul. Ecol.*, **51**: 65–81.

Kinnison, M.T. and Hendry, A.P. 2001. The pace of modern life II: from rates of contemporary microevolution to pattern and process. *Genetica*, **112/113**: 145–164.

Kisdi, É. and Geritz, S.A.H. 1999. Adaptive dynamics in allele space: evolution of genetic polymorphism by small mutations in a heterogeneous environment. *Evolution*, **53**: 993–1008.

Leimar, O. 2005. The evolution of phenotypic polymorphism: randomized strategies versus evolutionary branching. *Am. Nat.*, **165**: 669–681.

Leimar, O. 2009. Multidimensional convergence stability. *Evol. Ecol. Res.*, **11**: 191–208.

Losos, J.B. 2009. *Lizards in an Evolutionary Tree: Ecology and Adaptive Radiation of Anoles*. Berkeley, CA: University of California Press.

MacArthur, R. 1972. *Geographical Ecology*. New York: Harper & Row.

MacArthur, R. and Levins, R. 1967. The limiting similarity, convergence, and divergence of coexisting species. *Am. Nat.*, **101**: 377–385.

Matessi, C. and Di Pasquale, C. 1996. Long term evolution of multi-locus traits. *J. Math. Biol.*, **34**: 613–653.

Metz, J.A.J., Nisbet, R.M. and Geritz, S.A.H. 1992. How should we define 'fitness' for general ecological scenarios? *Trends Ecol. Evol.*, **7**: 198–202.

Metz, J.A.J., Geritz, S.A.H., Meszéna, G., Jacobs, F.J.A. and van Heerwaarden, J.S. 1996. Adaptive dynamics: a geometrical study of the consequences of nearly faithful reproduction. In *Stochastic and Spatial Structures of Dynamical Systems* (S.J. van Strien and S.M. Verduyn-Lunel, eds.), pp. 183–231. Amsterdam: North-Holland.

Payne, J.L., Mazzucco, R. and Dieckmann, U. 2011. The evolution of conditional dispersal and reproductive isolation along environmental gradients. *J. Theor. Biol.*, **273**: 147–155.

Ravigné, V., Dieckmann, U. and Olivieri, I. 2009. Live where you thrive: joint evolution of habitat choice and local adaptation facilitates specialization and promotes diversity. *Am. Nat.*, **174**: E141–E169.

Roughgarden, J. 1972. Evolution of niche width. *Am. Nat.*, **106**: 683–718.

Roughgarden, J. 1974. Species packing and the competition function with illustrations from coral reef fish. *Theor. Popul. Biol.*, **5**: 163–186.

Roughgarden, J. 1976. Resource partitioning among competing species: a coevolutionary approach. *Theor. Popul. Biol.*, **9**: 388–424.

Schluter, D. 2000. *The Ecology of Adaptive Radiation*. Oxford: Oxford University Press.

Seehausen, O. 2006. African cichlid fish: a model system in adaptive radiation research. *Proc. R. Soc. Lond. B*, **273**: 1987–1998.

Vukics, A., Asboth, J. and Meszéna, G. 2003. Speciation in multivariate evolutionary space. *Phys. Rev. E.*, **68**: 041903.

APPENDIX A: MUTATION PROBABILITY DISTRIBUTIONS

Here we explain how the mutation probability distributions used in our three examples are defined and interpreted in terms of mutational step sizes. For all three examples, we define the mutation probability distributions as bivariate normal distributions in the original coordinate system $\mathbf{S} = (X, Y)^{\mathrm{T}}$,

$$M(\boldsymbol{\delta}\mathbf{S}) = \exp\left(-\tfrac{1}{2}\,\boldsymbol{\delta}\mathbf{S}^{\mathrm{T}}\,\boldsymbol{\Lambda}^{-1}\,\boldsymbol{\delta}\mathbf{S}\right)/(2\pi\sqrt{\det\boldsymbol{\Lambda}}), \tag{A1a}$$

where $\boldsymbol{\Lambda}$ is the mutational variance–covariance matrix, given by

$$\boldsymbol{\Lambda} = \begin{pmatrix} \sigma_{\mathrm{X}}^2 & \sigma_{\mathrm{XY}}^2 \\ \sigma_{\mathrm{XY}}^2 & \sigma_{\mathrm{Y}}^2 \end{pmatrix} = \iint \begin{pmatrix} X^2 & XY \\ XY & Y^2 \end{pmatrix} M(\mathbf{S})\,\mathrm{d}X\mathrm{d}Y. \tag{A1b}$$

The two eigenvalues of the symmetric matrix $\boldsymbol{\Lambda}$ are real and give the maximum and minimum variances of mutational step sizes, and the two corresponding eigenvectors give the directions in which these extrema are attained.

For the first model, $\boldsymbol{\Lambda}$ is given by

$$\boldsymbol{\Lambda} = \mathbf{P}_{\boldsymbol{\Lambda}} \begin{pmatrix} \sigma_1^2 & 0 \\ 0 & \sigma_2^2 \end{pmatrix} \mathbf{P}_{\boldsymbol{\Lambda}}^{-1},$$

$$\mathbf{P}_{\boldsymbol{\Lambda}} = \frac{1}{\sqrt{2}} \begin{pmatrix} -1 & 1 \\ 1 & 1 \end{pmatrix} = \frac{1}{\sqrt{2}}\,(\mathbf{e}_1, \mathbf{e}_2), \tag{A2}$$

with $\sigma_1 \geq \sigma_2 > 0$. Accordingly, the standard deviation of mutational step sizes has its maximum σ_1 in the direction of $\mathbf{e}_1 = (-1, 1)^{\mathrm{T}}$, and its minimum σ_2 in the direction of $\mathbf{e}_2 = (1, 1)^{\mathrm{T}}$. For the second and third model, $\boldsymbol{\Lambda}$ is given by $((\sigma_{\mathrm{X}}^2, 0), (0, \sigma_{\mathrm{Y}}^2))^{\mathrm{T}}$, with $\sigma_{\mathrm{X}} \geq \sigma_{\mathrm{Y}} > 0$.

APPENDIX B: CONDITIONS FOR PROTECTED DIMORPHISMS FOR DISRUPTIVE SELECTION PARALLEL TO DIRECTIONAL SELECTION

Here we derive conditions for the emergence of protected dimorphisms along maximum-likelihood-invasion paths (MLIPs) for settings in which the maximum disruptive selection is parallel to directional selection in the locally normalized coordinate system. We first examine which mutants in such settings create maximum-likelihood invasions (MLI mutants), which then enables us to derive the aforementioned conditions.

We consider a locally normalized coordinate system $\mathbf{s} = (x, y)^{\mathrm{T}}$ with origin at $\mathbf{S}_0$, in which akin to equation (1) the normalized invasion-fitness function is expressed as

$$\begin{aligned} f(\mathbf{s}'; \mathbf{s}) = {} & G_{\mathbf{x}}\delta x + G_{\mathbf{y}}\delta y \\ & + \frac{1}{2} C_{\mathbf{xx}} x\delta x + \frac{1}{2} C_{\mathbf{yy}} y\delta y + \frac{1}{2} C_{\mathbf{xy}} x\delta y + \frac{1}{2} C_{\mathbf{yx}} y\delta x \\ & + \frac{1}{2} D_{\mathbf{xx}}\delta x^2 + \frac{1}{2} D_{\mathbf{yy}}\delta y^2. \end{aligned} \tag{B1a}$$

As before, we assume that $\mathbf{s}$ is under disruptive selection and that the strength of disruptive selection is maximal along the x-axis ($D_{\mathbf{xx}} > 0$).

We assume that the resident is located at the origin, $\mathbf{s} = (0, 0)^{\mathrm{T}}$, corresponding to $\mathbf{S}_0$, without loss of generality. Because directional selection is assumed to be parallel to the direction of maximum disruptive selection, we can infer that $G_{\mathbf{y}} = 0$. Then, $x, y = 0$ and equation (B1a) reduces to

$$f(\mathbf{s}'; \mathbf{s}) = G_{\mathbf{x}}\delta x + \frac{1}{2} D_{\mathbf{xx}}\delta x^2 + \frac{1}{2} D_{\mathbf{yy}}\delta y^2. \tag{B1b}$$

According to Dieckmann and Law (1996) and Ito and Dieckmann (submitted), at each invasion event the probability for mutant $\mathbf{s}'$ to invade resident $\mathbf{s}$ is given by

$$P(\mathbf{s}'; \mathbf{s}) = T\,\mu\hat{n}M(\boldsymbol{\delta}\mathbf{s})\,f(\mathbf{s}'; \mathbf{s})_+, \tag{B2a}$$

where T is a normalization ensuring $\int P(\mathbf{s}'; \mathbf{s})\,\mathrm{d}\mathbf{s}' = 1$, and the subscript '+' indicates the conversion of negative values h to 0. Below, we can omit this subscript since we focus on the maximum of $P(\mathbf{s}'; \mathbf{s})$, for which $f(\mathbf{s}'; \mathbf{s})$ always is positive. In this normalized trait space, the distribution $M(\boldsymbol{\delta}\mathbf{s})$ of mutational steps $\boldsymbol{\delta}\mathbf{s}$ is given by an isotropic bivariate normal distribution, $M(\boldsymbol{\delta}\mathbf{s}) = \mathrm{N}(\delta x, 0, \sigma^2)\mathrm{N}(\delta y, 0, \sigma^2)$. Substituting this and equation (B1b) into equation (B2a) yields

$$P(\mathbf{s}'; \mathbf{s}) = A \exp\left(-\frac{\delta x^2 + \delta y^2}{2\sigma^2}\right)\left[G_{\mathbf{x}}\delta x + \frac{1}{2} D_{\mathbf{xx}}\delta x^2 + \frac{1}{2} D_{\mathbf{yy}}\delta y^2\right], \tag{B2b}$$

where $A = \mu\hat{n}T/(2\pi\sigma^2)$. The mutant with maximum likelihood of invasion (MLI mutant), denoted by $\mathbf{s}'_{\mathrm{MLI}} = (x'_{\mathrm{MLI}}, y'_{\mathrm{MLI}})^{\mathrm{T}}$, maximizes $P(\mathbf{s}'; \mathbf{s})$. The mutational step taken by the MLI mutant is $\boldsymbol{\delta}\mathbf{s}_{\mathrm{MLI}} = (\delta x_{\mathrm{MLI}}, \delta y_{\mathrm{MLI}})^{\mathrm{T}} = \mathbf{s}'_{\mathrm{MLI}} - \mathbf{s}$. For convenience, we express mutational steps in polar coordinate $(\delta x, \delta y)^{\mathrm{T}} = (\varepsilon\cos\theta, \varepsilon\sin\theta)^{\mathrm{T}}$, which yields

$$P(\mathbf{s}';\mathbf{s}) = A\exp\left(-\frac{\varepsilon^2}{2\sigma^2}\right)\left[G_x\,\varepsilon\cos\theta + \frac{1}{2}D_{xx}\,\varepsilon^2\cos^2\theta + \frac{1}{2}D_{yy}\,\varepsilon^2\sin^2\theta\right]$$
$$= A\exp\left(-\frac{\varepsilon^2}{2\sigma^2}\right)\left[\frac{1}{2}D_{yy}\,\varepsilon^2 + \frac{1}{2}(D_{xx}-D_{yy})\varepsilon^2\cos^2\theta + G_{xx}\,\varepsilon\cos\theta\right]. \quad \text{(B2c)}$$

Note that $D_{xx} - D_{yy} > 0$, because disruptive selection is maximal in the direction of x. As $\cos\theta$ is maximal and mimimal at $\theta = 0$ and $\theta = \pi$, respectively, while $\cos^2\theta$ is maximal at $\theta = 0$ and $\theta = \pi$, the invasion probability above has its maximum at $\theta = 0$ for positive $G_{xx}\varepsilon$ and at $\theta = \pi$ for negative $G_{xx}\varepsilon$. Thus, the MLI mutant fulfils $\delta y_{MLI} = 0$ and δx_{MLI} is given by the δx that maximizes

$$P(\mathbf{s}';\mathbf{s}) = A\exp\left(-\frac{\delta x^2}{2\sigma^2}\right)\left[G_x\,\delta x + \frac{1}{2}D_{xx}\,\delta x^2\right]. \quad \text{(B2d)}$$

The terms above are symmetric with respect to the sign of δx, except for $G_x\delta x$. Therefore, when G_x is positive, $P(\mathbf{s}';\mathbf{s})$ for any negative δx is smaller than $P(\mathbf{s}';\mathbf{s})$ for a positive δx with the same absolute value. Thus, $\delta x_{MLI} > 0$ holds for $G_x > 0$. Analogously, $\delta x_{MLI} < 0$ holds for $G_x < 0$.

In addition, $\delta x = \delta x_{MLI}$ has to fulfil

$$\frac{\partial P(\mathbf{s}';\mathbf{s})}{\partial \delta x} = A\frac{1}{\sigma^2}\exp\left(-\frac{\delta x^2}{2\sigma^2}\right)\left[G_x(\sigma^2-\delta x^2) + \frac{1}{2}D_{xx}\,\delta x(2\sigma^2-\delta x^2)\right] = 0. \quad \text{(B3)}$$

For positive G_x, this requires $\sigma \le \delta x_{MLI} \le \sqrt{2}\sigma$ (because $D_{xx}\delta x_{MLI} > 0$, as D_{xx} is assumed to be positive and $\delta x_{MLI} > 0$ for $G_x > 0$). For negative, G_x, similarly, $-\sqrt{2}\sigma \le \delta x_{MLI} \le -\sigma$ is required (because then $D_{xx}\delta x_{MLI} < 0$). In summary, the MLI mutant thus always fulfils $\sigma \le |\delta x_{MLI}| \le \sqrt{2}\sigma$ and $\delta y_{MLI} = 0$.

On the basis of these features of MLI mutants, we now examine whether the MLI mutant and the considered resident can coexist. The conditions for protected dimorphism are given by conditions for mutual invasibility, $f(\mathbf{s}'_{MLI};\mathbf{s}) > 0$ and $f(\mathbf{s};\mathbf{s}'_{MLI}) > 0$. By substituting $\mathbf{s}'_{MLI} = (\delta x_{MLI} + x, y)^T$ and $x = y = 0$ into equation (B1a), these conditions are expressed as

$$f(\mathbf{s}'_{MLI};\mathbf{s}) = G_x\,\delta x_{MLI} + \frac{1}{2}D_{xx}\,\delta x_{MLI}^2 > 0, \quad \text{(B4a)}$$

and

$$f(\mathbf{s};\mathbf{s}'_{MLI}) = -G_x\,\delta x_{MLI} - \frac{1}{2}C_{xx}\,\delta x_{MLI}^2 + \frac{1}{2}D_{xx}\,\delta x_{MLI}^2 > 0. \quad \text{(B4b)}$$

If

$$C_{xx} < 0, \quad \text{(B5)}$$

a sufficient condition for inequalities (B4) to be fulfilled is given by

$$\frac{|\delta x_{MLI}|D_{xx}}{2|G_x|} > 1. \quad \text{(B6)}$$

As $\sigma \le |\delta x_{MLI}| \le \sqrt{2}\sigma$, a sufficient condition for this inequality to be fulfilled is given by

$$\frac{\sigma D_{xx}}{2|G_x|} > 1. \quad \text{(B7)}$$

APPENDIX C: IDENTIFIYING EVOLUTIONARY-BRANCHING LINES AND AREAS

General procedure

Here we explain how to identify evolutionary-branching lines and areas in an arbitrary trait space, according to Ito and Dieckmann (submitted). For checking conditions for evolutionary-branching lines in an arbitrary trait space $\mathbf{S}$, the vector $\mathbf{G}$ and the matrices $\mathbf{C}$ and $\mathbf{D}$ of the local normalized invasion-fitness function $f(\mathbf{s}'; \mathbf{s})$ are all that is needed. To obtain these vector and matrices, the trait space $\mathbf{S}$ is first transformed so that mutational steps become isotropic, and then it is further rotated so that $\mathbf{D}$ becomes diagonal. Specifically, $F(\mathbf{S}'; \mathbf{S})$ is approximated in the same way as the normalized invasion-fitness function, equation (1),

$$F(\mathbf{S}'; \mathbf{S}) = \check{\mathbf{G}}\,\boldsymbol{\delta}\mathbf{S} + \frac{1}{2}(\mathbf{S} - \mathbf{S}_0)^{\mathrm{T}}\check{\mathbf{C}}\,\boldsymbol{\delta}\mathbf{S} + \frac{1}{2}\boldsymbol{\delta}\mathbf{S}^{\mathrm{T}}\check{\mathbf{D}}\,\boldsymbol{\delta}\mathbf{S}, \tag{C1a}$$

where

$$\begin{aligned} \check{\mathbf{G}} &= \mathbf{F}_{\mathbf{S}'}, \\ \check{\mathbf{C}} &= 2(\mathbf{F}_{\mathbf{S}'\mathbf{S}'} + \mathbf{F}_{\mathbf{S}\mathbf{S}'}), \\ \check{\mathbf{D}} &= \mathbf{F}_{\mathbf{S}'\mathbf{S}'}, \end{aligned} \tag{C1b}$$

with

$$\begin{aligned} &\mathbf{F}_{\mathbf{S}'} = (F_{\mathbf{X}'} \quad F_{\mathbf{Y}'})_{\mathbf{S}'=\mathbf{S}=\mathbf{S}_0}, \\ &\mathbf{F}_{\mathbf{S}'\mathbf{S}'} = \begin{pmatrix} F_{\mathbf{X}'\mathbf{X}'} & F_{\mathbf{X}'\mathbf{Y}'} \\ F_{\mathbf{X}'\mathbf{Y}'} & F_{\mathbf{Y}'\mathbf{Y}'} \end{pmatrix}_{\mathbf{S}'=\mathbf{S}=\mathbf{S}_0}, \quad \mathbf{F}_{\mathbf{S}\mathbf{S}} = \begin{pmatrix} F_{\mathbf{X}\mathbf{X}} & F_{\mathbf{X}\mathbf{Y}} \\ F_{\mathbf{X}\mathbf{Y}} & F_{\mathbf{Y}\mathbf{Y}} \end{pmatrix}_{\mathbf{S}'=\mathbf{S}=\mathbf{S}_0}, \quad \mathbf{F}_{\mathbf{S}\mathbf{S}'} = \begin{pmatrix} F_{\mathbf{X}\mathbf{X}'} & F_{\mathbf{X}\mathbf{Y}'} \\ F_{\mathbf{Y}\mathbf{X}'} & F_{\mathbf{Y}\mathbf{Y}'} \end{pmatrix}_{\mathbf{S}'=\mathbf{S}=\mathbf{S}_0}, \end{aligned} \tag{C1c}$$

where F_{α} for $\alpha = \mathrm{X}'$, Y', X, Y and $F_{\alpha\beta}$ for α, $\beta = \mathrm{X}'$, Y', X, Y denote the first and second partial derivatives of $F(\mathbf{S}'; \mathbf{S})$ with respect to α and β, respectively.

By locally normalizing the trait space through an affine transformation, i.e. by substituting $\mathbf{S} - \mathbf{S}_0 = \mathbf{Q}^{\mathrm{T}}\mathbf{B}\mathbf{s}$ and $\boldsymbol{\delta}\mathbf{S} = \mathbf{Q}^{\mathrm{T}}\mathbf{B}\,\boldsymbol{\delta}\mathbf{s}$ into equation (C1a) and comparing with equation (1), we see that $\mathbf{G}$, $\mathbf{C}$, and $\mathbf{D}$ are given by

$$\begin{aligned} \mathbf{G} &= \check{\mathbf{G}}\mathbf{Q}^{\mathrm{T}}\mathbf{B}, \\ \mathbf{C} &= \mathbf{B}^{\mathrm{T}}\mathbf{Q}\check{\mathbf{C}}\mathbf{Q}^{\mathrm{T}}\mathbf{B}, \\ \mathbf{D} &= \mathbf{B}^{\mathrm{T}}\mathbf{Q}\check{\mathbf{D}}\mathbf{Q}^{\mathrm{T}}\mathbf{B}. \end{aligned} \tag{C2a}$$

The matrix $\mathbf{Q}$ describes the scaling of mutational step sizes to make them isotropic,

$$\mathbf{Q} = \frac{1}{\sigma}\begin{pmatrix} \sigma_{\mathrm{x}} & \sigma_{\mathbf{XY}}^2/\sigma_{\mathbf{X}} \\ 0 & \sqrt{\sigma_{\mathbf{X}}^2\sigma_{\mathbf{Y}}^2 - \sigma_{\mathbf{XY}}^4}/\sigma_{\mathbf{X}} \end{pmatrix}, \tag{C2b}$$

where $\sigma_{\mathbf{X}}^2$, $\sigma_{\mathbf{Y}}^2$, and $\sigma_{\mathbf{XY}}^2$ are the components of the mutational variance–covariance matrix $\boldsymbol{\Lambda}$, and σ^2 is the dominant eigenvalue of $\boldsymbol{\Lambda}$, measuring the maximum variance of mutational step sizes among all directions in trait spaces. The matrix $\mathbf{Q}$ can be obtained as the Cholesky decomposition of $\boldsymbol{\Lambda}/\sigma^2$, $\boldsymbol{\Lambda}/\sigma^2 = \mathbf{Q}^{\mathrm{T}}\mathbf{Q}$, with $\mathbf{Q}$ having upper-triangular form. The matrix $\mathbf{B}$ describes the rotation of the trait axes to align them with the direction of maximum disruptive selection,

$$\mathbf{B} = (\mathbf{v}_1, \mathbf{v}_2), \tag{C2c}$$

where $\mathbf{v}_1$ and $\mathbf{v}_2$ are the eigenvectors of $\mathbf{Q}\check{\mathbf{D}}\mathbf{Q}^{\mathrm{T}}$, ordered so that the corresponding eigenvalues fulfil $\lambda_1 > \lambda_2$, which makes $\mathbf{D}$ diagonal with $D_{\mathrm{xx}} > D_{\mathrm{yy}}$.

By substituting equations (C2) into the conditions for evolutionary-branching lines, equations (2a–c), the set of phenotypes $\mathbf{S}_0$ fulfilling those conditions is found, thus yielding the evolutionary-branching lines.

Illustrative example

Here we elaborate on the illustrative analysis of evolutionary-branching lines and areas around an evolutionary-branching point in the simple example briefly explained in the subsection 'Sizes and shapes of evolutionary-branching lines and areas' in the main text.

As explained there, we suppose that a trait space $\mathbf{S} = (X, Y)^{\mathrm{T}}$ possesses an evolutionary-branching point at its origin. For a point $\mathbf{S}_0$ close to the origin, the invasion-fitness function $F(\mathbf{S}'; \mathbf{S})$ can be expanded as shown in equation (C1a). By further expanding $\check{\mathbf{G}}$, $\check{\mathbf{C}}$, and $\check{\mathbf{D}}$ in terms of $\mathbf{S}_0$ around the origin, these are approximately given by

$$\check{\mathbf{G}} = \check{\check{\mathbf{G}}} + \mathbf{S}_0^{\mathrm{T}}\check{\check{\mathbf{C}}}, \quad \check{\mathbf{C}} = \check{\check{\mathbf{C}}}, \quad \text{and} \quad \check{\mathbf{D}} = \check{\check{\mathbf{D}}}, \tag{C3}$$

where $\check{\check{\mathbf{G}}}$, $\check{\check{\mathbf{C}}}$, and $\check{\check{\mathbf{D}}}$ denote the matrices $\check{\mathbf{G}}$, $\check{\mathbf{C}}$, and $\check{\mathbf{D}}$ at $\mathbf{S}_0 = (0, 0)^{\mathrm{T}}$, respectively. For the origin to be an evolutionarily singular point, $\check{\check{\mathbf{G}}} = \mathbf{0}$ is required. For the sake of illustration, we assume that $\check{\check{\mathbf{D}}} = ((D_{\mathrm{XX}}, 0), (0, D_{\mathrm{YY}}))^{\mathrm{T}}$, $D_{\mathrm{XX}} \geq D_{\mathrm{YY}}$, and $\check{\check{\mathbf{C}}} = ((C_{\mathrm{XX}}, 0), (0, C_{\mathrm{YY}}))^{\mathrm{T}}$. And for the origin to be an evolutionary-branching point, we assume that it is strongly convergence stable, $C_{\mathrm{XX}}, C_{\mathrm{YY}} < 0$, and that it is not evolutionarily stable, $D_{\mathrm{XX}} > 0$. In addition, we assume that mutational steps in the traits X and Y have no correlation, $\sigma_{\mathrm{XY}} = 0$, and are largest along the X-axis, $\sigma_{\mathrm{X}} \geq \sigma_{\mathrm{Y}}$. Then, the matrices $\mathbf{Q}$ and $\mathbf{B}$ are given by the constant matrices,

$$\mathbf{Q} = \begin{pmatrix} 1 & 0 \\ 0 & \sigma_{\mathrm{Y}}/\sigma_{\mathrm{X}} \end{pmatrix} \text{ and } \quad \mathbf{B} = \begin{pmatrix} 1 & 0 \\ 0 & 1 \end{pmatrix}, \tag{C4}$$

with $\sigma = \sigma_{\mathrm{x}}$. Substituting equations (C3) and (C4) into equations (C2a) yields

$$\begin{aligned} \mathbf{G} &= (G_{\mathrm{x}} \quad G_{\mathrm{y}}) = (C_{\mathrm{XX}}X_0 \quad rC_{\mathrm{YY}}Y_0), \\ \mathbf{C} &= \begin{pmatrix} C_{\mathrm{xx}} & C_{\mathrm{xy}} \\ C_{\mathrm{yx}} & C_{\mathrm{yy}} \end{pmatrix} = \begin{pmatrix} C_{\mathrm{XX}} & 0 \\ 0 & r^2C_{\mathrm{YY}} \end{pmatrix}, \\ \mathbf{D} &= \begin{pmatrix} D_{\mathrm{xx}} & D_{\mathrm{xy}} \\ D_{\mathrm{xy}} & D_{\mathrm{yy}} \end{pmatrix} = \begin{pmatrix} D_{\mathrm{XX}} & 0 \\ 0 & r^2D_{\mathrm{YY}} \end{pmatrix}, \end{aligned} \tag{C5}$$

with $r = \sigma_{\mathrm{Y}}/\sigma_{\mathrm{X}}$. Substituting equations (C5) into the conditions for evolutionary-branching lines and areas, equations (2) and (3a) then yield equations (4) and (5).

APPENDIX D: FUNCTIONAL RESPONSE IN SECOND AND THIRD MODELS

Here we explain how the functional response used in the second and third models is derived. Extending results by Beddington (1975) and DeAngelis *et al.* (1975), we start by deriving the functional response of phenotype $\mathbf{S}$ to resource type z,

$$g_{\mathbf{R}}(z, \mathbf{S}) = \phi(\mathbf{S}) A c(z, \mathbf{S}) e_{\mathbf{R}} R(z), \tag{D1a}$$

where $\phi(\mathbf{S})$ is the search effort per consumption effort, A is the total rate of consumption effort, and $c(z, \mathbf{S})$ describes the probability density of consumption effort over resource type z by phenotype $\mathbf{S}$ per unit of its biomass. Thus, $\phi(\mathbf{S}) A c(z, \mathbf{S})$ is the probability density of search effort per unit time invested on resource type z by phenotype $\mathbf{S}$ per unit of its biomass (search effort for short). As a first-order approximation, the encounter rate of phenotype $\mathbf{S}$ with resource type z is assumed to be proportional to this search effort and to the density $R(z)$ of resource type z, resulting in the proportionality constant $e_{\mathbf{R}}$.

The first-order approximation is also applied to the rate of interference competition experienced by phenotype $\mathbf{S}$ while consuming resource type z,

$$g_{\mathbf{C}}(z, \mathbf{S}) = \phi(\mathbf{S}) A c(z, \mathbf{S}) e_{\mathbf{C}} C(z), \tag{D1b}$$

which is thus assumed to be proportional to the search effort and to the total consumption effort $C(z)$ invested on resource type z by all phenotypes, with a proportionality constant $e_{\mathbf{C}}$. $C(z)$ is given by

$$C(z) = A \sum_{j=1}^{\mathbf{L}} n_j c(z, \mathbf{S}_j). \tag{D2}$$

The sum of energy invested into resource search, resource handling, and interference competition, measured in terms of rates and integrated over all resource types z, equals the total rate A of consumption effort,

$$\int \phi(\mathbf{S}) A c(z, \mathbf{S})\, \mathrm{d}z + \int h_{\mathbf{R}} g_{\mathbf{R}}(z, \mathbf{S})\, \mathrm{d}z + \int h_{\mathbf{C}} g_{\mathbf{C}}(z, \mathbf{S})\, \mathrm{d}z = A, \tag{D3}$$

where $h_{\mathbf{R}}$ and $h_{\mathbf{C}}$ scale the energy requirements for resource handling and interference competition relative to those for resource search. Here it is assumed that these relative energy requirements do not depend on resource type, and that they are not complicated by spatial population structure. Substituting equations (D1) into equation (D3) yields

$$\phi(\mathbf{S}) = \frac{1}{1 + h_{\mathbf{R}} e_{\mathbf{R}} \tilde{R}(\mathbf{S}) + h_{\mathbf{C}} e_{\mathbf{C}} \tilde{C}(\mathbf{S})}, \tag{D4}$$

and substituting this into equation (D1a) yields

$$g_{\mathbf{R}}(z, \mathbf{S}) = \frac{A c(z, \mathbf{S}) R(z)}{\alpha + \beta \tilde{R}(\mathbf{S}) + \gamma \tilde{C}(\mathbf{S})}, \tag{D5}$$

where

$$\tilde{R}(\mathbf{S}) = \int c(z, \mathbf{S}) R(z) \mathrm{d}z, \quad \tilde{C}(\mathbf{S}) = \int c(z, \mathbf{S}) C(z) \mathrm{d}z, \tag{D6}$$

$\alpha = 1/e_{\mathbf{R}}$, $\beta = h_{\mathbf{R}}$, and $\gamma = h_{\mathbf{C}} e_{\mathbf{C}} / e_{\mathbf{R}}$. Integrating equation (D4) over all resource types z, $g(\mathbf{S}) = \int g_{\mathbf{R}}(z, \mathbf{S})\, \mathrm{d}z$, finally yields the sought functional response,

$$g(\mathbf{S}) = \frac{A \tilde{R}(\mathbf{S})}{\alpha + \beta \tilde{R}(\mathbf{S}) + \gamma \tilde{C}(\mathbf{S})}. \tag{D7}$$

Here the parameters α, β, and γ measure the costs for resource search, resource handling, and interference competition, respectively.

APPENDIX E: INVASION FITNESS IN SECOND MODEL

Here we derive the invasion-fitness function for the second model. First, for the functional response in equation (D7), we need to specify the total amounts of resource and competitors encountered by phenotype $\mathbf{S}_i$, $\tilde{R}(\mathbf{S}_i)$ and $\tilde{C}(\mathbf{S}_i)$, which according to equation (D6) are given by the following overlap integrals,

$$\begin{aligned}\tilde{R}(\mathbf{S}_i) &= \int c(z, \mathbf{S}_i) R(z)\, \mathrm{d}z = R_0 \mathrm{N}(X_i, m_{\mathbf{R}},\ Y_i^2 + \sigma_{\mathbf{R}}^2),\\ \tilde{C}(\mathbf{S}_i) &= \int c(z, \mathbf{S}_i) C(z)\, \mathrm{d}z = A \sum\nolimits_{j=1}^{L} n_j \mathrm{N}(X_i,\ X_j,\ Y_i^2 + Y_j^2),\end{aligned} \tag{E1}$$

where $C(z)$ is the total consumption effort invested on resource type z by all phenotypes $\mathbf{S}_j$, as given by equation (D2).

Second, we describe the costs of specialization or generalization by an additional death rate that linearly varies with the niche width Y of a phenotype $\mathbf{S}$,

$$d(Y) = d_0 - d_1 Y, \tag{E2}$$

as specified by the two parameters d_0 and d_1: a positive d_1 results in a cost of specialization, whereas a negative d_1 results in a cost of generalization.

Third, for a monomorphic population with phenotype $\mathbf{S}$ and equilibrium biomass $\hat{n}$, the invasion fitness of a mutant with phenotype $\mathbf{S}'$ is then derived according to equation (7c) as

$$F(\mathbf{S}'; \mathbf{S}) = \lim_{n' \to 0} \frac{1}{n'} \frac{\mathrm{d}n'}{\mathrm{d}t} = \lambda g(\mathbf{S}') - d(Y'), \tag{E3a}$$

with $g(\mathbf{S}')$ as specified in equation (D7) with

$$\begin{aligned}\tilde{R}(\mathbf{S}') &= \mathrm{N}(X', m_{\mathbf{R}},\ Y'^2 + \sigma_R^2),\\ \tilde{C}(\mathbf{S}') &= A\hat{n}\mathrm{N}(X',\ X,\ Y'^2 + Y^2).\end{aligned} \tag{E3b}$$

APPENDIX F: INVASION FITNESS IN THIRD MODEL

Here we derive the invasion-fitness function for the third model. First, the total resource distribution is given by

$$R(z) = B(z) + \sum\nolimits_{j=1}^{L} n_j r(z, \mathbf{S}_j). \tag{F1a}$$

The rate of actual resource gain by phenotype $\mathbf{S}_i$ is then given by $g(\mathbf{S}_i)$ as specified in equation (D7) with

$$\begin{aligned}\tilde{R}(\mathbf{S}_i) &= \int c(z, \mathbf{S}_i) R(z)\, \mathrm{d}z = R_0 \mathrm{N}(X_i, m_{\mathbf{R}}, \sigma_{\mathrm{c}}^2 + \sigma_R^2) + \sum\nolimits_{j=1}^{L} n_j \mathrm{N}(X_i,\ Y_j, \sigma_{\mathrm{c}}^2 + \sigma_{\mathrm{r}}^2),\\ \tilde{C}(\mathbf{S}_i) &= \int c(z, \mathbf{S}_i) C(z)\, \mathrm{d}z = A \sum\nolimits_{j=1}^{L} n_j \mathrm{N}(X_i, X_j, 2\sigma_{\mathrm{c}}^2),\end{aligned} \tag{F1b}$$

according to equation (D6), where $C(z)$ is the total consumption effort invested on resource type z by all phenotypes $\mathbf{S}_j$, as given by equation (D2). By assuming that predators do not

distinguish phenotypes of prey when they share the same resource quality z, we obtain the functional response of phenotype $\mathbf{S}_i$ to $\mathbf{S}_j$ as $g(\mathbf{S}_i)$ multiplied by the fraction of $\mathbf{S}_j$ in the resources preyed upon by $\mathbf{S}_i$,

$$g_{\mathrm{p}}(\mathbf{S}_i, \mathbf{S}_j) = g(\mathbf{S}_i) \int c(z, \mathbf{S}_i) n_j r(z, \mathbf{S}_j)\, \mathrm{d}z / \tilde{R}(\mathbf{S}_i) = g(\mathbf{S}_i) n_j \mathrm{N}(X_i,\ Y_j,\ \sigma_{\mathrm{c}}^2 + \sigma_{\mathrm{r}}^2) / \tilde{R}(\mathbf{S}_i). \quad \text{(F1c)}$$

Second, the rate of biomass loss of phenotype $\mathbf{S}_i$ per its unit biomass is then given by

$$l(\mathbf{S}_i) = \frac{1}{n_i} \sum\nolimits_{j=1}^{L} n_j g_{\mathrm{p}}(\mathbf{S}_j, \mathbf{S}_i). \quad \text{(F2)}$$

Third, for a monomorphic population with phenotype $\mathbf{S}$ and equilibrium biomass $\hat{n}$, the invasion fitness of a mutant phenotype $\mathbf{S}'$ is then derived according to equation (8c) as

$$F(\mathbf{S}'; \mathbf{S}) = \lim_{n' \to 0} \frac{1}{n'} \frac{\mathrm{d}n'}{\mathrm{d}t} = \lambda g(\mathbf{S}') - \hat{n} g(\mathbf{S}) \mathrm{N}(X,\ Y', \sigma_{\mathrm{c}}^2 + \sigma_{\mathrm{r}}^2) / \tilde{R}(\mathbf{S}) - d \quad \text{(F3a)}$$

with

$$\tilde{R}(\mathbf{S}') = \mathrm{N}(X', m_{\mathbf{R}}, \sigma_{\mathrm{c}}^2 + \sigma_{\mathbf{R}}^2) + \hat{n} \mathrm{N}(X',\ Y, \sigma_{\mathrm{c}}^2 + \sigma_{\mathrm{r}}^2),$$
$$\tilde{C}(\mathbf{S}') = A \hat{n} \mathrm{N}(X', X, \sigma_{\mathrm{c}}^2). \quad \text{(F3b)}$$